Comparison of different degenerated approaches for the modeling of composite shell structures

Philippe Vidal, L. Gallimard, Olivier Polit

P. Vidal, L. Gallimard, O. Polit. Comparison of different degenerated approaches for the modeling of composite shell structures.
Finite Elements in Analysis and Design, Volume 195, 2021.

https://doi.org/10.1016/j.finel.2021.103585.

1. Introduction

The increasing use of composite material, in particular for curved structures, has led to the intensive development of appropriate two-dimensional shell theories that can accurately describe the response of multilayered anisotropic shells. In fact, the use of three-dimensional modelisation allows us to compute accurate local solutions, but, unfortunately, it is not well suitable due to prohibitive computational costs.

Two main ways are considered to obtain shell FE: (i) the "pure shell model" in which the displacement is associated with the local curvilinear vectors, and strain and stress are deduced using differential geometry [1,2]; (ii) the shell-like solid approach [3] where the displacement vector is defined in the global cartesian frame and jacobian matrix transformation is used to express strain and stress with respect to reference frame defined on the middle surface in order to introduce the constitutive law. In this approach, differentiation is simplified and the curvatures are not directly calculated [4]. It is widely used in commercial software for simplicity reasons. Considering anisotropic structures where 3D phenomena occur, it is also needed to develop enriched theories. According to published research, various approaches based on the Finite Element (FE) method for composite shells have been carried out. In the following, most of the mentioned works refer to the pure shell model. Thus, two families of models [5] can be identified:

- the Equivalent Single Layer (ESL) Models: It includes the most common theories, namely the classical Shell Theory (CST/Koïter) and First Order Shear Deformation Theory (FSDT/Nagdhi). The reader can refer to Ref. [6] for a description of the assumptions on the strain to derive different shell models. CST leads to inaccurate results for composites because both transverse shear and normal strains are neglected. In this way, shallow laminated shells are modelized in Refs. [7–9]. FSDT is the most popular model due to the possibility to use a C^0 FE, but it needs shear correction factors and transverse normal strain is always neglected, e.g. Ref. [10]. So, Higher-order Shear Deformation Theories (HSDT) have been developed to overcome these drawbacks. Various theories are proposed based on 7 ([11,12]) or 9 parameters [13]. Wide range of theories based on the Carrera's Unified Formulation are also addressed in Ref. [14]. In the ESL context, a simple way to improve the estimation of the mechanical quantities consists in adding zig-zag functions (Murakami [15,16]) in the displacement to introduce the slope discontinuity at the interface between two adjacent layers. It allows to describe the so-called zig-zag effect. It has been carried out by Brank [17] with a 7 parameters model. See also the work of Bhaskar [18] based on a HSDT approach.

- the Layer-Wise Models (LWM): the expression of the displace-ments/stresses can be written over each layer. Thus, the number of unknowns depends on the number of layers. A quadratic triangle element based on a constant shear angle is considered in Ref. [19], but a shear correction factor is needed. A three-dimensional shell element is proposed in Ref. [20]. A LW triangle FE is developed in Ref. [21] with a condensation technique at the pre-processing level. Ref. [22]. deals with a hybrid strain flat triangular FE based on the Hellinger-Reissner variational principle. Note that the trans-verse normal and shear stresses are only taken into account in Ref. [23] where a four-node isoparametric assumed strain is considered. We can mention the eight-node 3D hybrid-EAS solid shell element based on the Hu-Washizu variational principle in Ref. [24]. See also the previously mentioned work [14].

As an alternative, refined models have been developed in order to improve the accuracy of ESL models avoiding the additional computational cost of LW approach. Based on physical considerations and after some algebraic transformations, the number of unknowns becomes independent of the number of layers. We can mention the work of Yasin [25] including 5 parameters dedicated to shallow shells. Shariyat [26] has also developed a so-called zig-zag model including 15 parameters. It should be also mentioned the work of Dau [2] where a C^1 triangular six-node FE (Argyris-Ganev) based on the Sinus model is considered involving 5 parameters. The approach ensures the continuity conditions of the transverse shear stresses at the interfaces between two adjacent layers.

For the present topics, it should be noted that the mentioned works are based on the Finite Element method for linear elasticity problem in mechanics and applied to laminated composites, knowing that many other approaches (meshless, analytical, semi-analytical …) are involved in open literature. Furthermore, the fundamental subject about the shear and membrane locking of shell is not addressed here. So, this above literature deals with only some aspects of the broad research activity about composite shells. An extensive assessment of different approaches for both various theories and/or finite element applications can be found in Refs. [27–34].

The main goal of this work consists in assessing two new degenerated shell approaches to model any laminated composite structures. For the transverse coordinate, a fourth-order z-expansion in each layer is used as it is well suited for this type of structures [35]. The first approach is based on the classical Layer-Wise model [5,16] where the number of unknowns per node depends on the number of layers. The linear problem is directly solved. The originality of this approach is the conjunction of this classical LW model with the degenerated shell model. The second one implies the so-called Proper Generalized Decomposition (PGD) [36–39] as it has shown interesting features in the reduction model framework. In particular, it has been applied for composite shells in Refs. [40–43]. However, these studies are either dedicated to cylindrical shell geometry or not well suited to model composite structures. The present approach is based on the separation representation where the displacements are written under the form of a sum of products of bidimensional polynomials of (x_1, x_2) and unidimensional polynomials of z. The deduced non-linear problem is solved using a fixed point strategy in which the resolution of two linear problems is carried out alternatively. This process yields to a 2D and a 1D problems in which the number of unknowns is smaller than the previous Layerwise approach.

This article is organized as follows. First, the geometry of the shell-like solid is described including the reference frames. The general problem to be solved is precised. Then, the two involved approches, namely the LW model and PGD method, are described in the particular framework of the degenerated shell model. For the latter, the particular assumption on the displacements yields a non-linear problem solved by a fixed point strategy. The FE discretization is also described and finally, numerical tests are performed. The present approaches are assessed on different shell configurations. Deep and shallow shells, different slenderness ratios and stacking sequences are considered for various boundary conditions. The limitations and advantages of the models are precised and comparison with reference solutions are given.

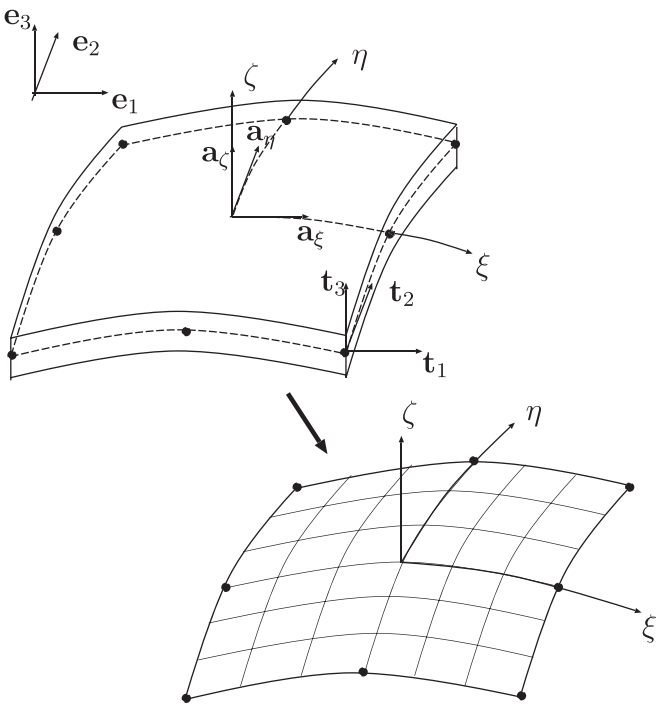

Fig. 1. Description of the geometry of the 8-node shell element.

2. Description of the shell

This preliminary section is dedicated to the geometric description of the shell-like solid and to the different reference frames that will be used to construct the finite shell element.

2.1. Description of the geometry

Let us consider a shell $\mathcal{C} = \Omega \times [-\frac{e}{2}, \frac{e}{2}]$ where e is the constant thickness of the shell and Ω is the middle surface. The description of the geometry of the shell is based on the Cartesian coordinates of the nodes and on the finite element approximation over the elementary domain. For this, an eight-node quadrilateral finite element is used. Fig. 1 illustrates the employed finite element approximation and shows the different reference frames to describe the geometry and the mechanics of the shell-like body. These different bases are precised in Table 1. The global coordinates of any arbitrary point in the elementary domain can be expressed in terms of the reduced (curvilinear) coordinates ξ, η and the rectilinear normal coordinate z:

$$\mathbf{\Phi}(\xi,\eta,z) = \begin{bmatrix} X_1(\xi,\eta,z) \\ X_2(\xi,\eta,z) \\ X_3(\xi,\eta,z) \end{bmatrix} = \sum_{i=1}^{8} N_{q_i}(\xi,\eta) \begin{bmatrix} X_1 \\ X_2 \\ X_3 \end{bmatrix}_i + z \sum_{i=1}^{8} N_{q_i}(\xi,\eta) \begin{bmatrix} t_{31} \\ t_{32} \\ t_{33} \end{bmatrix}_i \quad (1)$$

where $N_{q_i}(\xi,\eta)$ are the classical Serendipity interpolation functions.

The thickness of the shell is described in terms of the unit vector $\mathbf{t}_3 = \begin{bmatrix} t_{31} & t_{32} & t_{33} \end{bmatrix}^T$ normal to the middle surface Ω. We prescribe $\mathbf{t}_3 = \mathbf{a}_3$, i.e., the normal direction of the local curvilinear reference frame on Ω coincides with the normal direction of the local tangent plane to Ω (see Fig. 1). The covariant in-plane base vectors $\mathbf{a}_\alpha$ are usually obtained from the map $\mathbf{\Phi}$ introduced in Eq. (1) to define the shell mid-surface Ω:

Table 1
Reference frames used for the description of the shell.

$(\mathbf{e}_1, \mathbf{e}_2, \mathbf{e}_3)$	Direct orthonormal Cartesian basis, (G)
(X_1, X_2, X_3)	Global Cartesian coordinates, (G)
$(\mathbf{t}_1, \mathbf{t}_2, \mathbf{t}_3)$	Direct orthonormal local basis, plane tangent to Ω, **local (L)**
$(x_1, x_2, x_3 = z)$	Local curvilinear coordinates on Ω, **local (L)**
$(\mathbf{a}_1, \mathbf{a}_2, \mathbf{a}_3)$	Reduced local basis, plane tangent to Ω, **Reduced (R)**
(ξ, η)	Reduced curvilinear coordinates on Ω, **Reduced (R)**

$$\mathbf{a}_\alpha = \mathbf{\Phi}(\xi, \eta, z)_{,\alpha} \quad \text{for } \alpha = \xi, \eta \tag{2}$$

and the normal vector $\mathbf{t}_3 = \mathbf{a}_3$ is finally obtained from the perpendicularity condition:

$$\mathbf{t}_3 = \mathbf{a}_3 = \frac{\mathbf{a}_1 \wedge \mathbf{a}_2}{\|\mathbf{a}_1 \wedge \mathbf{a}_2\|} \tag{3}$$

The construction of the local base vectors $\mathbf{t}_1$ and $\mathbf{t}_2$ follows the procedure suggested by Ref. [3].

2.2. The change of bases

The displacement field vector is expressed with respect to the global reference frame $\mathbf{e}_i$ as

$$\mathbf{u}(X_1, X_2, X_3) = \sum_{i=1}^{3} u_i^G(X_1, X_2, X_3)\mathbf{e}_i \tag{4}$$

where the superscript G indicates that the components are taken in the global reference frame. The displacement vector $\mathbf{u} = [u_1\, u_2\, u_3]^T$ is expressed in the local orthonormal basis (L) by

$$\mathbf{u}^L = \left[T_{LG}\right]\ \mathbf{u}^G \text{ with } \left[T_{LG}\right] = \begin{bmatrix} t_{11} & t_{12} & t_{13} \\ t_{21} & t_{22} & t_{23} \\ t_{31} & t_{32} & t_{33} \end{bmatrix} = \begin{bmatrix} \mathbf{t}_1 \cdot \mathbf{e}_1 & \mathbf{t}_1 \cdot \mathbf{e}_2 & \mathbf{t}_1 \cdot \mathbf{e}_3 \\ \mathbf{t}_2 \cdot \mathbf{e}_1 & \mathbf{t}_2 \cdot \mathbf{e}_2 & \mathbf{t}_2 \cdot \mathbf{e}_3 \\ \mathbf{t}_3 \cdot \mathbf{e}_1 & \mathbf{t}_3 \cdot \mathbf{e}_2 & \mathbf{t}_3 \cdot \mathbf{e}_3 \end{bmatrix} \tag{5}$$

In the same way, the following expression can be obtained:

$$\mathbf{u}^G = \left[T_{GL}\right]\ \mathbf{u}^L \quad \text{with} \quad \left[T_{GL}\right] = \left[T_{LG}\right]^{-1} = \left[T_{LG}\right]^T = \begin{bmatrix} t_{11} & t_{21} & t_{31} \\ t_{12} & t_{22} & t_{32} \\ t_{13} & t_{23} & t_{33} \end{bmatrix} \tag{6}$$

The displacement vector $\mathbf{u}^R$ defined in the reduced local basis is constructed as

$$\mathbf{u}^R = \left[T_{RG}\right]\ \mathbf{u}^G \quad \text{with} \quad \left[T_{RG}\right] = \begin{bmatrix} a_{11} & a_{21} & a_{31} \\ a_{12} & a_{22} & a_{32} \\ a_{13} & a_{23} & a_{33} \end{bmatrix} = \begin{bmatrix} \mathbf{a}_1 \cdot \mathbf{e}_1 & \mathbf{a}_1 \cdot \mathbf{e}_2 & \mathbf{a}_1 \cdot \mathbf{e}_3 \\ \mathbf{a}_2 \cdot \mathbf{e}_1 & \mathbf{a}_2 \cdot \mathbf{e}_2 & \mathbf{a}_2 \cdot \mathbf{e}_3 \\ \mathbf{a}_3 \cdot \mathbf{e}_1 & \mathbf{a}_3 \cdot \mathbf{e}_2 & \mathbf{a}_3 \cdot \mathbf{e}_3 \end{bmatrix} \tag{7}$$

Furthermore, the inverse relation holds:

$$\mathbf{u}^G = \left[T_{GR}\right]\ \mathbf{u}^R \qquad \text{with} \qquad \left[T_{GR}\right] = \left[T_{RG}\right]^{-1} \tag{8}$$

Similar relations can be established between the local orthonormal L and reduced R reference frames by substituting G by L.

3. Reference problem description

3.1. The weak form of the boundary value problem

The shell is submitted to a surface force density $\mathbf{t}$ defined over a subset $\partial\boldsymbol{C}_F$ of the boundary. We assume that a prescribed displacement $\mathbf{u} = \mathbf{u}_d$ is imposed on $\Gamma_D = \partial\boldsymbol{C} - \partial\boldsymbol{C}_F$. The mechanical problem is based on the variational principle which is given by:

find $\mathbf{u}(M) \in U$ (space of admissible displacements) such that

$$a(\mathbf{u}, \delta\mathbf{u}) = b(\delta\mathbf{u}), \quad \forall\delta\mathbf{u} \in \delta U \tag{9}$$

with

$$\begin{aligned} a(\mathbf{u}, \delta\mathbf{u}) &= \iiint_{\boldsymbol{C}} \delta\boldsymbol{\varepsilon}^{L^T}\boldsymbol{\sigma}^L \; d\boldsymbol{C} \\ b(\delta\mathbf{u}) &= \iint_{\partial\boldsymbol{C}_F} \delta\mathbf{u} \cdot \mathbf{t} \; d\partial\boldsymbol{C} \end{aligned}$$

where U is the space of admissible displacements, i.e. $U = \{\mathbf{u} \in (H^1(\mathcal{V}))^3 / \mathbf{u} = \mathbf{u}_d \text{ on } \Gamma_D\}$. We have also $\delta U = \{\mathbf{u} \in (H^1(\mathcal{V}))^3 / \mathbf{u} = 0 \text{ on } \Gamma_D\}$.

For the present work, $\partial\boldsymbol{C}_F$ is considered as the top or bottom surface of the shell, that is $z = z_F$ with $z_F = \pm e/2$. For sake of clarity, the body forces are neglected in the developments.

3.2. The constitutive relation

The stress tensor is obtained from the strain tensor using the constitutive equations. All these tensors will be referred to the local basis vectors associated with the middle surface of the shell. In case of laminated shells composed of NC perfectly bonded orthotropic plies, the three-dimensional constitutive law of the kth layer in the local orthonormal basis is expressed by:

$$\boldsymbol{\sigma}^{L(k)} = \mathbf{C}^{(k)}\boldsymbol{\varepsilon}^{L(k)} \tag{10}$$

For convenience reasons, stresses $\boldsymbol{\sigma}$ and strains $\boldsymbol{\varepsilon}$ are split into three groups:

$$\begin{aligned} \boldsymbol{\sigma}_p^T &= [\sigma_{11}\ \sigma_{22}\ \tau_{12}], \quad \boldsymbol{\sigma}_s^T = [\tau_{13}\ \tau_{23}], \quad \boldsymbol{\sigma}_n = \sigma_{33} \\ \boldsymbol{\varepsilon}_p^T &= [\varepsilon_{11}\ \varepsilon_{22}\ \gamma_{12}], \quad \boldsymbol{\varepsilon}_s^T = [\gamma_{13}\ \gamma_{23}], \quad \boldsymbol{\varepsilon}_n = \varepsilon_{33} \end{aligned} \tag{11}$$

where the subscripts p, n and s denote in-plane, transverse normal and shear values, respectively.

Using the separation between the different components described above, the three dimensional constitutive law of the kth layer is given by:

$$\begin{cases} \boldsymbol{\sigma}_p^{(k)} = \mathbf{Q}_{pp}^{(k)}\boldsymbol{\varepsilon}_p^{(k)} + \mathbf{Q}_{pn}^{(k)}\boldsymbol{\varepsilon}_n^{(k)} \\ \boldsymbol{\sigma}_n^{(k)} = \mathbf{Q}_{np}^{(k)}\boldsymbol{\varepsilon}_p^{(k)} + Q_{33}^{(k)}\boldsymbol{\varepsilon}_n^{(k)} \\ \boldsymbol{\sigma}_s^{(k)} = \mathbf{Q}_s^{(k)}\boldsymbol{\varepsilon}_s^{(k)} \end{cases} \tag{12}$$

where

$$\mathbf{Q}_{pp}^{(k)} = \begin{bmatrix} Q_{11}^{(k)} & Q_{12}^{(k)} & Q_{16}^{(k)} \\ Q_{12}^{(k)} & Q_{22}^{(k)} & Q_{26}^{(k)} \\ Q_{16}^{(k)} & Q_{26}^{(k)} & Q_{66}^{(k)} \end{bmatrix} \quad \mathbf{Q}_{pn}^{(k)} = \mathbf{Q}_{np}^{(k)T} = \begin{bmatrix} Q_{13}^{(k)} \\ Q_{23}^{(k)} \\ Q_{36}^{(k)} \end{bmatrix} \quad \mathbf{Q}_s^{(k)} = \begin{bmatrix} Q_{55}^{(k)} & Q_{45}^{(k)} \\ Q_{45}^{(k)} & Q_{44}^{(k)} \end{bmatrix} \tag{13}$$

where $Q_{ij}^{(k)}$ are the three-dimensional stiffness coefficients of the layer (k).

3.3. The strain

The compatible strain field is obtained from the linear strain-displacement relations, which in the global reference frame read

$$\varepsilon_{ij}^{G}\left(\mathbf{u}^{G}\right)=\frac{1}{2}\left(\mathbf{u}_{,i}^{G}+\mathbf{u}_{j}^{G}\right) \tag{14}$$

where $i,j = X_1,X_2,X_3$. The components of the strain tensor can be calculated with respect to the three bases G, L and R:

$$\varepsilon(\mathbf{u}^{G})=\varepsilon_{ij}^{G}(\mathbf{e}^{i}\otimes\mathbf{e}^{j})=\varepsilon_{ij}^{L}(\mathbf{t}^{i}\otimes\mathbf{t}^{j})=\varepsilon^{R\,ij}(\mathbf{a}_{i}\otimes\mathbf{a}_{j})=\varepsilon_{ij}^{R}(\mathbf{a}^{i}\otimes\mathbf{a}^{j}) \tag{15}$$

It must be noted that covariant and contravariant components are the same in an orthonormal basis, for example $\mathbf{e}_i$ and $\mathbf{t}_i$. This is not the case when the strain components are expressed in the local reduced reference frame $\mathbf{a}_i$. Therefore, we can express the strain tensor in the reduced basis in either covariant or contravariant components.

In this work, strain components are first calculated with respect to the local reduced base vectors, using FE approximations. Then, using tensorial transformation, they are expressed with respect to the local cartesian base vectors, in order to take into account the constitutive equations. Therefore, the local cartesian base vectors must be chosen as reference frame and introduced in the variational formulation.

For this purpose, we have

$$\epsilon_{ij}^{L}=\epsilon_{kl}^{R}\,(\mathbf{a}^{k}.\mathbf{t}_{i})\,(\mathbf{a}^{l}.\mathbf{t}_{j}) \tag{16}$$

This tensorial transformation can be written under matrix product form, for the following components (11, 22, 12), using the transformation matrix denoted $[TT_{LR}]$. The transformation between local and reduced for the third index (3 or z) is 1, because same unit vector is used.

The expression of this transformation is obtained from:

$$\left[T_{LR}\right]=\left[T_{RL}\right]^{-1}\ \text{with}\ \left[T_{RL}\right]=\begin{bmatrix}\mathbf{a}_1.\mathbf{t}_1 & \mathbf{a}_1.\mathbf{t}_2\\ \mathbf{a}_2.\mathbf{t}_1 & \mathbf{a}_2.\mathbf{t}_2\end{bmatrix} \tag{17}$$

and using tensorial matrix of order two which have the following expression:

$$\left[TT_{LR}\right]=\begin{bmatrix} T_{LR}(1,1)^2 & T_{LR}(1,2)^2 & T_{LR}(1,1)\,T_{LR}(1,2)\\ T_{LR}(2,1)^2 & T_{LR}(2,2)^2 & T_{LR}(2,1)\,T_{LR}(2,2)\\ 2\,T_{LR}(1,1)\,T_{LR}(2,1) & 2\,T_{LR}(1,2)\,T_{LR}(2,2) & T_{LR}(1,1)\,T_{LR}(2,2)+T_{LR}(1,2)\,T_{LR}(2,1)\end{bmatrix} \tag{18}$$

Finally, we have to calculate the strain in the reduced local basis. In this local basis, coordinates denoted $(1,2)$ are in fact (ξ,η) due to the use of FE approximation.

We have

$$\epsilon_{ij}^{R}=\frac{1}{2}\left(\mathbf{u}_{,i}^{L}\,.\,\mathbf{a}_{j}+\mathbf{u}_{j}^{L}\,.\,\mathbf{a}_{i}\right) \tag{19}$$

and

$$\mathbf{u}_{,i}^{L}\,.\,\mathbf{a}_{j}=u_{k,i}^{L}\,(\mathbf{t}_{k}\,.\,\mathbf{a}_{j})+u_{k}^{L}\,(\mathbf{t}_{k,j}\,.\,\mathbf{a}_{i}) \tag{20}$$

In this last expression, the second term needs to use differential geometry of shell in order to express derivatives of the base vectors. In the following, it is neglected in order to simplify the numerical implementation.

4. First approach: classical LW model with degenerated shell approach

In this section, the classical LW approach is briefly recalled as it is widely developed in open literature [5,16]. Hereafter, the developments are focused on the framework of our degenerated shell approach.

The fourth-order expansion of the displacement in the kth layer is expressed as

$$\mathbf{u}^{L(k)}=\begin{bmatrix}u_1^{(k)}(x_1,x_2,z)\\ u_2^{(k)}(x_1,x_2,z)\\ u_3^{(k)}(x_1,x_2,z)\end{bmatrix}=\sum_{j=1}^{5}f_{LW}^{j}(z)\begin{bmatrix}u_j^{(k)}(x_1,x_2)\\ v_j^{(k)}(x_1,x_2)\\ w_j^{(k)}(x_1,x_2)\end{bmatrix} \tag{21}$$

where $f_{LW}^{j}(z)$ are Lagrangian interpolation functions. $u_j^{(k)},v_j^{(k)},w_j^{(k)}$ are defined in Ω.

Using this expression to compute the strains in conjunction with the changes of basis described in Section 3.3 and introducing them in Eq. (9) with a FE approximation, it drives to a classical linear system to be solved as

$$\mathbf{K_{LW}}\mathbf{q}^{LW}=\boldsymbol{\mathcal{F}}_{\mathbf{LW}} \tag{22}$$

where $\boldsymbol{K_{LW}}$ and $\boldsymbol{\mathcal{F}}_{\mathbf{LW}}$ are the rigidity matrix and the force vector of the LW approach, $\mathbf{q}^{LW}$ contains all the unknown degrees of freedom. The expression of the classical elementary matrices before the assembly process is not given for brevity reason.

At each node, the number of unknowns depends on the number of layers, $N_{dofnode}^{LW}=3.(4.N_z+1)$, where N_z is the number of numerical layers. Thus, the size of the system increases with N_z as $N_{LW}=3.(4.N_z+1).(3.N_x.N_y+2(N_x+N_y)+1)$. N_xxN_y are the number of elements in the ξ and η directions, respectively.

5. Second approach: application of the Proper Generalized Decomposition to degenerated shell model

In this section, the application of the PGD is developed for the present degenerated shell analysis. This work is an extension of the previous studies on shell structures ([42,43]) to take into account any geometrical composite shells.

5.1. The displacement

The displacement solution is constructed as the sum of N products of functions of in-plane coordinates and transverse coordinate ($N\in\mathbb{N}$ is the order of the representation) in the global basis:

$$\mathbf{u}^{G}=\begin{bmatrix}u_1(x_1,x_2,z)\\ u_2(x_1,x_2,z)\\ u_3(x_1,x_2,z)\end{bmatrix}=\sum_{j=1}^{N}\begin{bmatrix}f_1^{j}(z)\,v_1^{j}(x_1,x_2)\\ f_2^{j}(z)\,v_2^{j}(x_1,x_2)\\ f_3^{j}(z)\,v_3^{j}(x_1,x_2)\end{bmatrix} \tag{23}$$

where (f_1^j,f_2^j,f_3^j) are defined in Ω_z and (v_1^j,v_2^j,v_3^j) are defined in Ω. Ω and Ω_z are bi-dimensional domain associated with the mid-surface of the shell, and the unidimensional domain associated with the normal fiber respectively.

In this paper, a classical eight-node FE approximation is used in Ω and a LW description is chosen in Ω_z as it is particularly suitable for the modeling of composite structure.

5.2. The problem to be solved

Now, we briefly recall the process to build the different terms (couples) involving in Eq. (23). Classically, the resolution of Eq. (9) is based

on a greedy algorithm. If we assume that the first m functions have been already computed, the trial function for the iteration $m+1$ is written as

$$\mathbf{u}^{m+1} = \mathbf{u}^m + \begin{bmatrix} f_1\, v_1 \\ f_2\, v_2 \\ f_3\, v_3 \end{bmatrix} = \mathbf{u}^m + \mathbf{f} \circ \mathbf{v} \tag{24}$$

where the "$\circ$" operator stands for Hadamard's element-wise product, (v_1, v_2, v_3) and (f_1, f_2, f_3) are the functions to be computed and $\mathbf{u}^m$ is the associated known set at iteration m defined by

$$\mathbf{u}^m = \sum_{i=1}^{m} \begin{bmatrix} f_1^i\, v_1^i \\ f_2^i\, v_2^i \\ f_3^i\, v_3^i \end{bmatrix} \tag{25}$$

The test functions are

$$\delta(\mathbf{f} \circ \mathbf{v}) = \delta\mathbf{f} \circ \mathbf{v} + \delta\mathbf{v} \circ \mathbf{f} \tag{26}$$

with

$$\mathbf{v} = \begin{bmatrix} v_1 \\ v_2 \\ v_3 \end{bmatrix} \mathbf{f} = \begin{bmatrix} f_1 \\ f_2 \\ f_3 \end{bmatrix} \tag{27}$$

Introducing the test function defined by Eq. (26) and the trial function defined by Eq. (24) into the weak form Eq. (9), the two following equations to be solved can be deduced:

- for the test function $\delta\mathbf{f}$

$$a(\mathbf{v} \circ \mathbf{f}, \mathbf{v} \circ \delta\mathbf{f}) = b(\mathbf{v} \circ \delta\mathbf{f}) - a(\mathbf{u}^m, \mathbf{v} \circ \delta\mathbf{f}) \quad \forall \delta\mathbf{f} \tag{28}$$

- for the test function $\delta\mathbf{v}$

$$a(\mathbf{f} \circ \mathbf{v}, \mathbf{f} \circ \delta\mathbf{v}) = b(\mathbf{f} \circ \delta\mathbf{v}) - a(\mathbf{u}^m,\ \mathbf{f} \circ \delta\mathbf{v}) \quad \forall \delta\mathbf{v} \tag{29}$$

The bilinear form a can be written under the following form using Eq. (12)

$$\begin{aligned} a(\mathbf{u}, \delta\mathbf{u}) = \int_C & \delta\boldsymbol{\varepsilon}_p^{L\,T} \left(\mathbf{Q}_{pp}^{(k)} \boldsymbol{\varepsilon}_p^L + \mathbf{Q}_{pn}^{(k)} \boldsymbol{\varepsilon}_n^L \right) + \delta\boldsymbol{\varepsilon}_n^{L\,T} \left(\mathbf{Q}_{np}^{(k)} \boldsymbol{\varepsilon}_p^L + Q_{33}^{(k)} \boldsymbol{\varepsilon}_n^L \right) \\ & + \delta\boldsymbol{\varepsilon}_s^{L\,T} \mathbf{Q}_s^{(k)} \boldsymbol{\varepsilon}_s^L \; dC \end{aligned} \tag{30}$$

This expression has to be written in the suitable form depending on the two problems Eq. (28) and Eq. (29).

This coupled non-linear problem is solved using a classical strategy based on a fixed point method. For each problem, only unknown 1D or 2D function has to be found. So, the approach leads to the process given in Algorithm 1. The fixed point algorithm is stopped when the distance between two consecutive terms are sufficiently small (Cf. [35]).

Algorithm 1 Classical algorithm

for $m = 0$ to N_{max} **do**
  Initialize $\widetilde{\mathbf{v}}^{(0)}$
  for $k = 1$ to k_{max} **do**
    Compute $\widetilde{\mathbf{f}}^{(k)}$ from Eq. (28) (linear equation on Ω_z), $\widetilde{\mathbf{v}}^{(k-1)}$ being known
    Compute $\widetilde{\mathbf{v}}^{(k)}$ from Eq. (29) (linear equation on Ω), $\widetilde{\mathbf{f}}^{(k)}$ being known
    Check for convergence
  end for
  Set $\mathbf{f}^{m+1} = \widetilde{\mathbf{f}}^{(k)}$, $\mathbf{v}^{m+1} = \widetilde{\mathbf{v}}^{(k)}$
  Set $\mathbf{u}^{m+1} = \mathbf{u}^m + \mathbf{f}^{m+1} \circ \mathbf{v}^{m+1}$
  Check for convergence
end for

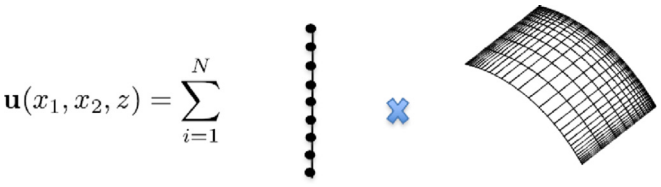

Fig. 2. discretization of the displacements for the PGD method.

5.3. Finite element discretization

In this section, the shell finite element approximation is built. For the present approach, the computation of the discretized displacements relies on 2 meshes, as shown in Fig. 2. The first one is 1D with 3 unknowns par node related to the discretization of the z-functions $f_1(z), f_2(z), f_3(z)$. It is possible to choose different interpolation orders. That will determine the number of nodes of the 1D mesh. For instance, a fourth-order expansion with NC layers implies $4.NC + 1$ nodes (considering one element per physical layer). The second one is 2D with 3 unknowns per node related to the discretization of the in-plane functions $v_1(x_1, x_2), v_2(x_1, x_2), v_3(x_1, x_2)$. Thus, considering any points on the middle plane of the shell structure, the computations of the displacements through the thickness depend on the same N z-functions. The unknown functions of z are global for the whole shell.

In this work, a discrete representation of the functions $(\mathbf{v}, \mathbf{f})$ is introduced, using (i) a classical eight-node shell finite element approximation in Ω, (ii) Lagrange interpolations in Ω_z. The elementary vector of degrees of freedom (dof) associated with one element Ω_e of the mesh in Ω is denoted $\mathbf{q}_e^v$. The vector of dofs associated with the expansion in Ω_z is denoted $\mathbf{q}^f$. The displacement field is determined from the values of $\mathbf{q}_e^v$ and $\mathbf{q}_e^f$ by

$$\mathbf{v}_e = \mathbf{N}_\xi \mathbf{q}_e^v,\ \mathbf{f}_e = \mathbf{N}_z \mathbf{q}_e^f \tag{31}$$

The matrices $\mathbf{N}_\xi$, $\mathbf{N}_z$ contain the interpolation functions.

5.4. Finite element problem to be solved on Ω

For the sake of simplicity, the function $\widetilde{\mathbf{f}}^{(k)}$ which is assumed to be known, will be denoted $\widetilde{\mathbf{f}}$, and the function $\widetilde{\mathbf{v}}^{(k)}$ to be computed will be denoted $\mathbf{v}$. Using the particular form of the displacement Eq. (23) in Eq. (19) and the FE approximation for v and f, the reduced in-plane, normal and shear strains can be deduced under the following form:

$$\begin{cases} \boldsymbol{\varepsilon}_p^R(\widetilde{f}\, v) & = \boldsymbol{\Sigma}_z^{\mathbf{p}}(\widetilde{f})\ \mathbf{BeseTA_p}\ \mathbf{q}_e^v \\ \boldsymbol{\varepsilon}_n^R(\widetilde{f}\, v) & = \boldsymbol{\Sigma}_z^{\mathbf{n}}(\widetilde{f})\ \mathbf{BeseTA_n}\ \mathbf{q}_e^v \\ \boldsymbol{\varepsilon}_s^R(\widetilde{f}\, v) & = \left[\boldsymbol{\Sigma}_z^{\mathbf{s1}}(\widetilde{f})\ \mathbf{BeseTA_{s1}} + \boldsymbol{\Sigma}_z^{\mathbf{s3}}(\widetilde{f})\ \mathbf{BeseTA_{s3}} \right] \mathbf{q}_e^v \end{cases} \tag{32}$$

where $\mathbf{BeseTA}_p$, $\mathbf{BeseTA}_n$ and $\mathbf{BeseTA}_{s1}$, $\mathbf{BeseTA}_{s3}$ contain the shape functions, their derivatives, the scalar products $\mathbf{t}_i \cdot \mathbf{a}_i$ and $\mathbf{t}_i \cdot \mathbf{e}_i$. Their expressions and those of $\boldsymbol{\Sigma}_z^{\mathbf{p}}$, $\boldsymbol{\Sigma}_z^{\mathbf{n}}$, $\boldsymbol{\Sigma}_z^{\mathbf{s1}}$, $\boldsymbol{\Sigma}_z^{\mathbf{s3}}$ are given in A.1.

Using Eq. (32) and Eq. (16) in the expression Eq. (30), the discretization of the bilinear form a in the weak formulation given in Eq. (29) can be deduced:

$$
\begin{aligned}
a(\mathbf{u},\delta\mathbf{u}) = \sum_e \int_{\Omega_e}\int_{\Omega_z} \delta\mathbf{q}_e^{\nu T} \\
&\Big\{ \mathbf{BaseTA_p}^T\, \boldsymbol{\Sigma}_{\mathbf{z}}^{\mathbf{p}}(\widetilde{f})^T\, \mathbf{TT}_{LR}^T\, \mathbf{Q}_{pp}^{(k)}\, \mathbf{TT}_{LR}\, \boldsymbol{\Sigma}_{\mathbf{z}}^{\mathbf{p}}(\widetilde{f})\, \mathbf{BaseTA_p} \\
&+ \mathbf{BaseTA_p}^T\, \boldsymbol{\Sigma}_{\mathbf{z}}^{\mathbf{p}}(\widetilde{f})^T\, \mathbf{TT}_{LR}^T\, \mathbf{Q}_{pn}^{(k)}\, \boldsymbol{\Sigma}_{\mathbf{z}}^{\mathbf{n}}(\widetilde{f})\, \mathbf{BaseTA_n} \\
&+ \mathbf{BaseTA_n}^T\, \boldsymbol{\Sigma}_{\mathbf{z}}^{\mathbf{n}}(\widetilde{f})^T\, \mathbf{Q}_{np}^{(k)}\, \mathbf{TT}_{LR}\, \boldsymbol{\Sigma}_{\mathbf{z}}^{\mathbf{p}}(\widetilde{f})\, \mathbf{BaseTA_p} \\
&+ \mathbf{BaseTA_n}^T\, \boldsymbol{\Sigma}_{\mathbf{z}}^{\mathbf{n}}(\widetilde{f})^T\, Q_{33}^{(k)}\, \boldsymbol{\Sigma}_{\mathbf{z}}^{\mathbf{n}}(\widetilde{f})\, \mathbf{BaseTA_n} \\
&+ \left[\boldsymbol{\Sigma}_{\mathbf{z}}^{\mathbf{s1}}(\widetilde{f})\, \mathbf{BaseTA_{s1}} + \boldsymbol{\Sigma}_{\mathbf{z}}^{\mathbf{s3}}(\widetilde{f})\, \mathbf{BaseTA_{s3}}\right]^T \mathbf{T}_{LR}^T \\
&\mathbf{Q}_{ss}^{(k)}\, \mathbf{T}_{LR}\, \left[\boldsymbol{\Sigma}_{\mathbf{z}}^{\mathbf{s1}}(\widetilde{f})\, \mathbf{BaseTA_{s1}} + \boldsymbol{\Sigma}_{\mathbf{z}}^{\mathbf{s3}}(\widetilde{f})\, \mathbf{BaseTA_{s3}}\right] \Big\}\, \mathbf{q}_e^{\nu}\, d\Omega_z\, d\Omega_e
\end{aligned}
\tag{33}
$$

To split the integration with respect to the midsurface and the z-coordinate, it is needed to write the three matrix products $\mathbf{TT}_{LR}\, \boldsymbol{\Sigma}_{\mathbf{z}}^{\mathbf{p}}(\widetilde{f})$, $\mathbf{T}_{LR}\, \boldsymbol{\Sigma}_{\mathbf{z}}^{\mathbf{s1}}(\widetilde{f})$ and $\mathbf{T}_{LR}\, \boldsymbol{\Sigma}_{\mathbf{z}}^{\mathbf{s3}}(\widetilde{f})$ in Eq. (33) under a specific form $\mathbf{M_1}(\widetilde{f})\mathbf{M_2}$. Thus, we introduce these new expressions as

$$
\begin{cases}
\mathbf{TT}_{LR}\, \boldsymbol{\Sigma}_{\mathbf{z}}^{\mathbf{p}}(\widetilde{f}) & = \boldsymbol{\Sigma}_{\mathbf{new}}^{\mathbf{p}}(\widetilde{f})\, \mathbf{MM}_{LR}^{p} \\
\mathbf{T}_{LR}\, \boldsymbol{\Sigma}_{\mathbf{z}}^{\mathbf{s1}}(\widetilde{f}) & = \boldsymbol{\Sigma}_{\mathbf{new}}^{\mathbf{s1}}(\widetilde{f})\, \mathbf{M}_{LR}^{s1} \\
\mathbf{T}_{LR}\, \boldsymbol{\Sigma}_{\mathbf{z}}^{\mathbf{s3}}(\widetilde{f}) & = \boldsymbol{\Sigma}_{\mathbf{new}}^{\mathbf{s3}}(\widetilde{f})\, \mathbf{M}_{LR}^{s3}
\end{cases}
\tag{34}
$$

Only the expressions of $\boldsymbol{\Sigma}_{\mathbf{new}}^{\mathbf{p}}(\widetilde{f})$ and $\mathbf{MM}_{LR}^{p}$ are given in A.2. The same type can be deduced for $\boldsymbol{\Sigma}_{\mathbf{new}}^{\mathbf{s1}}(\widetilde{f})$, $\boldsymbol{\Sigma}_{\mathbf{new}}^{\mathbf{s3}}(\widetilde{f})$, $\mathbf{M}_{LR}^{s1}$ and $\mathbf{M}_{LR}^{s3}$

Introducing these new expressions in Eq. (33), a can be advantageously expressed as follows

$$
\begin{aligned}
a(\mathbf{u},\delta\mathbf{u}) = \sum_e \int_{\Omega_e} \delta\mathbf{q}_e^{\nu T} \Big\{ &\mathbf{BaseTA_p}^T\, \mathbf{MM}_{LR}^{p\ T}\, \mathbf{k}_{\mathbf{z}}^{\mathbf{pp}}(\widetilde{f})\, \mathbf{MM}_{LR}^{p}\, \mathbf{BaseTA_p} \\
&+ \mathbf{BaseTA_p}^T\, \mathbf{MM}_{LR}^{p\ T}\, \mathbf{k}_{\mathbf{z}}^{\mathbf{pn}}(\widetilde{f})\, \mathbf{BaseTA_n} \\
&+ \mathbf{BaseTA_n}^T\, \mathbf{k}_{\mathbf{z}}^{\mathbf{np}}(\widetilde{f})\, \mathbf{MM}_{LR}^{p}\, \mathbf{BaseTA_p} \\
&+ \mathbf{BaseTA_n}^T\, \mathbf{k}_{\mathbf{z}}^{\mathbf{33}}(\widetilde{f})\, \mathbf{BaseTA_n} \\
&+ \mathbf{BaseTA_{s1}}^T\, \mathbf{M}_{LR}^{s1\ T}\, \boldsymbol{k}_{\mathbf{z}}^{\boldsymbol{s11}}(\widetilde{f})\, \mathbf{M}_{LR}^{s1}\, \mathbf{BaseTA_{s1}} \\
&+ \mathbf{BaseTA_{s1}}^T\, \mathbf{M}_{LR}^{s1\ T}\, \boldsymbol{k}_{\mathbf{z}}^{\boldsymbol{s13}}(\widetilde{f})\, \mathbf{M}_{LR}^{s3}\, \mathbf{BaseTA_{s3}} \\
&+ \mathbf{BaseTA_{s3}}^T\, \mathbf{M}_{LR}^{s3\ T}\, \boldsymbol{k}_{\mathbf{z}}^{\boldsymbol{s31}}(\widetilde{f})\, \mathbf{M}_{LR}^{s1}\, \mathbf{BaseTA_{s1}} \\
&+ \mathbf{BaseTA_{s3}}^T\, \mathbf{M}_{LR}^{s3\ T}\, \boldsymbol{k}_{\mathbf{z}}^{\boldsymbol{s33}}(\widetilde{f})\, \mathbf{M}_{LR}^{s3}\, \mathbf{BaseTA_{s3}} \Big\}\, \mathbf{q}_e^{\nu} d\Omega_e
\end{aligned}
\tag{35}
$$

with

$$
\begin{aligned}
\mathbf{k}_{\mathbf{z}}^{\mathbf{pp}}(\widetilde{f}) &= \int_{\Omega_z} \boldsymbol{\Sigma}_{\mathbf{new}}^{\mathbf{p}}(\widetilde{f})^T\, \mathbf{Q}_{pp}^{(k)}\, \boldsymbol{\Sigma}_{\mathbf{new}}^{\mathbf{p}}(\widetilde{f}) dz \\
\mathbf{k}_{\mathbf{z}}^{\mathbf{pn}}(\widetilde{f}) &= \int_{\Omega_z} \boldsymbol{\Sigma}_{\mathbf{new}}^{\mathbf{p}}(\widetilde{f})^T\, \mathbf{Q}_{pn}^{(k)}\, \boldsymbol{\Sigma}_{\mathbf{z}}^{\mathbf{n}}(\widetilde{f}) dz \\
\mathbf{k}_{\mathbf{z}}^{\mathbf{np}}(\widetilde{f}) &= \mathbf{k}_{\mathbf{z}}^{\mathbf{pn}}(\widetilde{f})^T \\
\mathbf{k}_{\mathbf{z}}^{\mathbf{33}}(\widetilde{f}) &= \int_{\Omega_z} \boldsymbol{\Sigma}_{\mathbf{z}}^{\mathbf{n}}(\widetilde{f})^T\, Q_{33}^{(k)}\, \boldsymbol{\Sigma}_{\mathbf{z}}^{\mathbf{n}}(\widetilde{f}) dz \\
\boldsymbol{k}_{\mathbf{z}}^{\boldsymbol{s11}}(\widetilde{f}) &= \int_{\Omega_z} \boldsymbol{\Sigma}_{\mathbf{new}}^{\mathbf{s1}}(\widetilde{f})^T\, \mathbf{Q}_{ss}^{(k)}\, \boldsymbol{\Sigma}_{\mathbf{new}}^{\mathbf{s1}}(\widetilde{f}) dz \\
\boldsymbol{k}_{\mathbf{z}}^{\boldsymbol{s13}}(\widetilde{f}) &= \int_{\Omega_z} \boldsymbol{\Sigma}_{\mathbf{new}}^{\mathbf{s1}}(\widetilde{f})^T\, \mathbf{Q}_{ss}^{(k)}\, \boldsymbol{\Sigma}_{\mathbf{new}}^{\mathbf{s3}}(\widetilde{f}) dz \\
\boldsymbol{k}_{\mathbf{z}}^{\boldsymbol{s33}}(\widetilde{f}) &= \int_{\Omega_z} \boldsymbol{\Sigma}_{\mathbf{new}}^{\mathbf{s3}}(\widetilde{f})^T\, \mathbf{Q}_{ss}^{(k)}\, \boldsymbol{\Sigma}_{\mathbf{new}}^{\mathbf{s3}}(\widetilde{f}) dz \\
\boldsymbol{k}_{\mathbf{z}}^{\boldsymbol{s31}}(\widetilde{f}) &= \boldsymbol{k}_{\mathbf{z}}^{\boldsymbol{s13}}(\widetilde{f})^T
\end{aligned}
\tag{36}
$$

Note that the calculation of Eq. (36) is performed using an analytical integration.

Using Eq. (35), the variational problem defined on Ω from Eq. (29) leads to the linear system

$$
\mathbf{K}_{\mathbf{z}}(\widetilde{f})\mathbf{q}^{\nu} = \boldsymbol{\mathcal{R}}_{\mathbf{v}}(\widetilde{f}, u^n) \tag{37}
$$

where $\mathbf{K}_{\mathbf{z}}(\widetilde{f})$ is deduced from Eq. (35) and $\mathbf{q}^{\nu}$ is the vector of the nodal displacements in the global basis. The right hand side of Eq. (29) is not given for brevity reason. The same discretization process is used to deduce it.

5.5. Finite element problem to be solved on Ω_z

For the sake of simplicity, the function $\widetilde{\mathbf{v}}^{(k-1)}$ which is assumed to be known, will be denoted $\widetilde{\mathbf{v}}$, and the function $\widetilde{\mathbf{f}}^{(k)}$ to be computed will be denoted $\mathbf{f}$.

Using the particular form of the displacement Eq. (23) in Eq. (19) and the FE approximation for v and f, the three parts of the strains can be conveniently written under the following form:

$$
\begin{cases}
\boldsymbol{\epsilon}_p^R(\widetilde{\mathbf{v}}f) & = \boldsymbol{\Sigma}_{\mathbf{xy}}^{\mathbf{p}}(\widetilde{\nu})\, \mathbf{BaseNz}\, \mathbf{q}_e^f \\
\boldsymbol{\epsilon}_n^R(\widetilde{\mathbf{v}}f) & = \boldsymbol{\Sigma}_{\mathbf{xy}}^{\mathbf{n}}(\widetilde{\nu})\, \mathbf{BaseBz}\, \mathbf{q}_e^f \\
\boldsymbol{\epsilon}_s^R(\widetilde{\mathbf{v}}f) & = \boldsymbol{\Sigma}_{\mathbf{xy}}^{\mathbf{s1}}(\widetilde{\nu})\, \mathbf{BaseNz}\, \mathbf{q}_e^f + \boldsymbol{\Sigma}_{\mathbf{xy}}^{\mathbf{s3}}(\widetilde{\nu})\, \mathbf{BaseBz}\, \mathbf{q}_e^f
\end{cases}
\tag{38}
$$

where **BaseNz** and **BaseBz** contain the shape functions and their derivatives. Their expressions and those of $\boldsymbol{\Sigma}_{\mathbf{xy}}^{\mathbf{p}}(\widetilde{\nu})$, $\boldsymbol{\Sigma}_{\mathbf{xy}}^{\mathbf{n}}(\widetilde{\nu})$, $\boldsymbol{\Sigma}_{\mathbf{xy}}^{\mathbf{s1}}(\widetilde{\nu})$, $\boldsymbol{\Sigma}_{\mathbf{xy}}^{\mathbf{s3}}(\widetilde{\nu})$ are given in B.

Starting from the problem to be solved Eq. (28), Eq. (38) and Eq. (16) can be introduced to deduce the expression of a:

$$
\begin{aligned}
a(\mathbf{v}\circ\mathbf{f}, \mathbf{v}\circ\delta\mathbf{f}) = \sum_e \int_{\Omega_e^z}\int_{\Omega} \delta\mathbf{q}_e^{fT} \\
&\Big\{ \mathbf{BaseNz}^T\, \boldsymbol{\Sigma}_{\mathbf{xy}}^{\mathbf{p}}(\widetilde{\nu})^T\, \mathbf{TT}_{LR}^T\, \mathbf{Q}_{pp}^{(k)}\, \mathbf{TT}_{LR}\, \boldsymbol{\Sigma}_{\mathbf{xy}}^{\mathbf{p}}(\widetilde{\nu})\, \mathbf{BaseNz} \\
&+ \mathbf{BaseNz}^T\, \boldsymbol{\Sigma}_{\mathbf{xy}}^{\mathbf{p}}(\widetilde{\nu})^T\, \mathbf{TT}_{LR}^T\, \mathbf{Q}_{pn}^{(k)}\, \boldsymbol{\Sigma}_{\mathbf{xy}}^{\mathbf{n}}(\widetilde{\nu})\, \mathbf{BaseBz} \\
&+ \mathbf{BaseBz}^T\, \boldsymbol{\Sigma}_{\mathbf{xy}}^{\mathbf{n}}(\widetilde{\nu})^T\, \mathbf{Q}_{np}^{(k)}\, \mathbf{TT}_{LR}\, \boldsymbol{\Sigma}_{\mathbf{xy}}^{\mathbf{p}}(\widetilde{\nu})\, \mathbf{BaseNz} \\
&+ \mathbf{BaseBz}^T\, \boldsymbol{\Sigma}_{\mathbf{xy}}^{\mathbf{n}}(\widetilde{\nu})^T\, Q_{33}^{(k)}\, \boldsymbol{\Sigma}_{\mathbf{xy}}^{\mathbf{n}}(\widetilde{\nu})\, \mathbf{BaseBz} \\
&+ \left[\boldsymbol{\Sigma}_{\mathbf{xy}}^{\mathbf{s1}}(\widetilde{\nu})\, \mathbf{BaseNz} + \boldsymbol{\Sigma}_{\mathbf{xy}}^{\mathbf{s3}}(\widetilde{\nu})\, \mathbf{BaseBz}\right]^T \mathbf{T}_{LR}^T \\
&\mathbf{Q}_{ss}^{(k)}\, \mathbf{T}_{LR}\, \left[\boldsymbol{\Sigma}_{\mathbf{xy}}^{\mathbf{s1}}(\widetilde{\nu})\, \mathbf{BaseNz} + \boldsymbol{\Sigma}_{\mathbf{xy}}^{\mathbf{s3}}(\widetilde{\nu})\, \mathbf{BaseBz}\right] \Big\}\, \mathbf{q}_e^f d\Omega d\Omega_e^z
\end{aligned}
\tag{39}
$$

By integrating with respect to the in-plane coordinate, Eq. (39) becomes

$$
\begin{aligned}
a(\mathbf{v}\circ\mathbf{f}, \mathbf{v}\circ\delta\mathbf{f}) = \sum_e \delta\mathbf{q}_e^{fT} \int_{\Omega_e^z} \Big\{ &\mathbf{BaseNz}^T\, \mathbf{k}_{\mathbf{xy}}^{\mathbf{pp}(k)}(\widetilde{\nu})\, \mathbf{BaseNz} \\
&+ \mathbf{BaseNz}^T\, \mathbf{k}_{\mathbf{xy}}^{\mathbf{pn}(k)}(\widetilde{\nu})\, \mathbf{BaseBz} \\
&+ \mathbf{BaseBz}^T\, \mathbf{k}_{\mathbf{xy}}^{\mathbf{np}(k)}(\widetilde{\nu})\, \mathbf{BaseNz} \\
&+ \mathbf{BaseBz}^T\, \mathbf{k}_{\mathbf{xy}}^{\mathbf{33}(k)}(\widetilde{\nu})\, \mathbf{BaseBz} \\
&+ \mathbf{BaseNz}^T\, \boldsymbol{k}_{\boldsymbol{xy}}^{\boldsymbol{s11}(k)}(\widetilde{\nu})\, \mathbf{BaseNz} \\
&+ \mathbf{BaseNz}^T\, \boldsymbol{k}_{\boldsymbol{xy}}^{\boldsymbol{s13}(k)}(\widetilde{\nu})\, \mathbf{BaseBz} \\
&+ \mathbf{BaseBz}^T\, \boldsymbol{k}_{\boldsymbol{xy}}^{\boldsymbol{s31}(k)}(\widetilde{\nu})\, \mathbf{BaseNz} \\
&+ \mathbf{BaseBz}^T\, \boldsymbol{k}_{\boldsymbol{xy}}^{\boldsymbol{s33}(k)}(\widetilde{\nu})\, \mathbf{BaseBz} \Big\}\, d\Omega_e^z\, \mathbf{q}_e^f
\end{aligned}
\tag{40}
$$

with

$$
\begin{aligned}
\mathbf{k}_{xy}^{pp(k)}(\widetilde{\nu}) &= \int_{\Omega} \boldsymbol{\Sigma}_{xy}^{p}(\widetilde{\nu})^{T}\, \mathbf{TT}_{LR}^{T}\, \mathbf{Q}_{pp}^{(k)}\, \mathbf{TT}_{LR}\, \boldsymbol{\Sigma}_{xy}^{p}(\widetilde{f}) d\Omega \\
\mathbf{k}_{xy}^{pn(k)}(\widetilde{\nu}) &= \int_{\Omega} \boldsymbol{\Sigma}_{xy}^{p}(\widetilde{\nu})^{T}\, \mathbf{TT}_{LR}^{T}\, \mathbf{Q}_{pn}^{(k)}\, \boldsymbol{\Sigma}_{xy}^{n}(\widetilde{\nu}) d\Omega \\
\mathbf{k}_{xy}^{np(k)}(\widetilde{\nu}) &= \mathbf{k}_{z}^{pn(k)}(\widetilde{f})^{T} \\
\mathbf{k}_{xy}^{33(k)}(\widetilde{\nu}) &= \int_{\Omega} \boldsymbol{\Sigma}_{xy}^{n}(\widetilde{\nu})^{T}\, Q_{33}^{(k)}\, \boldsymbol{\Sigma}_{xy}^{n}(\widetilde{\nu}) d\Omega \\
\boldsymbol{k}_{xy}^{s11(k)}(\widetilde{\nu}) &= \int_{\Omega} \boldsymbol{\Sigma}_{xy}^{s1}(\widetilde{\nu})^{T} \mathbf{T}_{LR}^{T}\, \mathbf{Q}_{ss}^{(k)}\, \mathbf{T}_{LR}\, \boldsymbol{\Sigma}_{xy}^{s1}(\widetilde{\nu}) d\Omega \\
\boldsymbol{k}_{xy}^{s13(k)}(\widetilde{\nu}) &= \int_{\Omega} \boldsymbol{\Sigma}_{xy}^{s1}(\widetilde{\nu})^{T} \mathbf{T}_{LR}^{T}\, \mathbf{Q}_{ss}^{(k)}\, \mathbf{T}_{LR}\, \boldsymbol{\Sigma}_{xy}^{s3}(\widetilde{\nu}) d\Omega \\
\boldsymbol{k}_{xy}^{s33(k)}(\widetilde{\nu}) &= \int_{\Omega} \boldsymbol{\Sigma}_{xy}^{s3}(\widetilde{\nu})^{T} \mathbf{T}_{LR}^{T}\, \mathbf{Q}_{ss}^{(k)}\, \mathbf{T}_{LR}\, \boldsymbol{\Sigma}_{xy}^{s3}(\widetilde{\nu}) d\Omega \\
\boldsymbol{k}_{xy}^{s31(k)}(\widetilde{\nu}) &= \boldsymbol{k}_{xy}^{s13(k)}(\widetilde{\nu})^{T}
\end{aligned}
\tag{41}
$$

After an assembling procedure, Eq. (40) can be reported in Eq. (28) to deduce a linear system to be solved:

$$
\mathbf{K}_{xy}(\widetilde{\nu})\mathbf{q}^{f} = \mathcal{R}_{\mathbf{f}}(\widetilde{\nu}, u^{n}) \tag{42}
$$

where $\mathbf{K}_{xy}(\widetilde{\nu})$ is deduced from Eq. (40) and $\mathbf{q}^{f}$ is the vector of the nodal unknowns associated to $\mathbf{f}$. The right hand side of Eq. (28) is not given for brevity reason. The same discretization process is used to obtain it.

6. Numerical results

In this section, an eight-node quadrilateral FE based on the Serendipity interpolation functions is used for the unknowns depending on the in-plane coordinates. The geometry of the shell is approximated by this classical FE in the parametric space. A Gaussian numerical integration with 3×3 points is used to evaluate the elementary matrices.

We have developed two different degenerated shell approaches assuming a fourth-order z-expansion through each layer: (i) the first one, denoted LD4-S, is based on the LD4 model, as developed in the systematic work of Carrera and his "Carrera's Unified Formulation" (CUF), see Refs. [16,44,45]. In the latter, 12NC + 3 unknown functions per node are used in this kinematic; (ii) the second one, denoted VS-LD4-S, is based on the variable separation approach (PGD), the number of unknowns is reduced to three per node for the 1D and 2D models. The results are compared with an approach based on an exact geometry description using LD4 model. It is denoted LD4-M. In the subsequent examples, this model can be considered as a reference solution. As the same assumptions on the shell geometry are used for both LD4-S and VS-LD4-S models, the comparison between these two models allows us to evaluate only the error associated to the variable separation part.

Several static tests are presented in order to validate our approaches and evaluate their efficiencies. For each of them, a preliminary convergence study has been carried out to fix the suitable mesh. Only the first one is presented for conciseness reason. Different boundary conditions, geometries and number of layers are addressed to assess the present approaches and highlight the possibilities and limitations.

For the numerical simulations related to the PGD model, two simultaneous couples are first computed and the following ones are built one by one. This strategy is needed to achieve the convergence of the method.

6.1. Simply-supported cylindrical shell

The first test case is based on a configuration proposed by Ren [46]. It concerns a semi-infinite simply-supported cylindrical shell submitted to a constant pressure. It is described below:

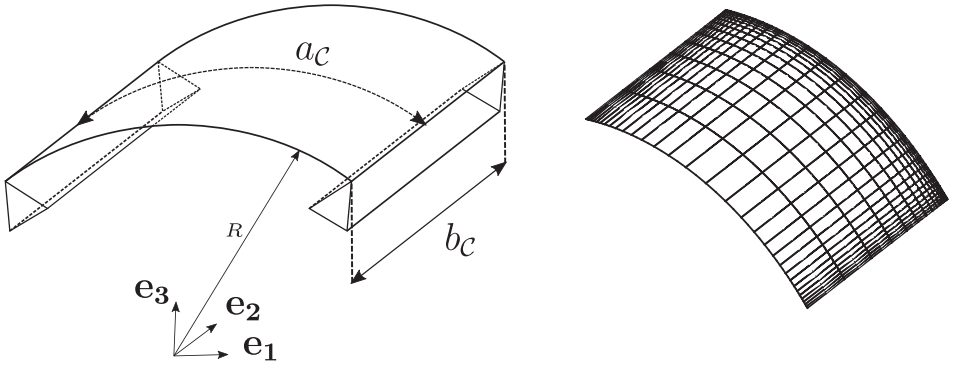

Fig. 3. Simply supported cylindrical shell (left) - mesh of a quarter of the structure (right).

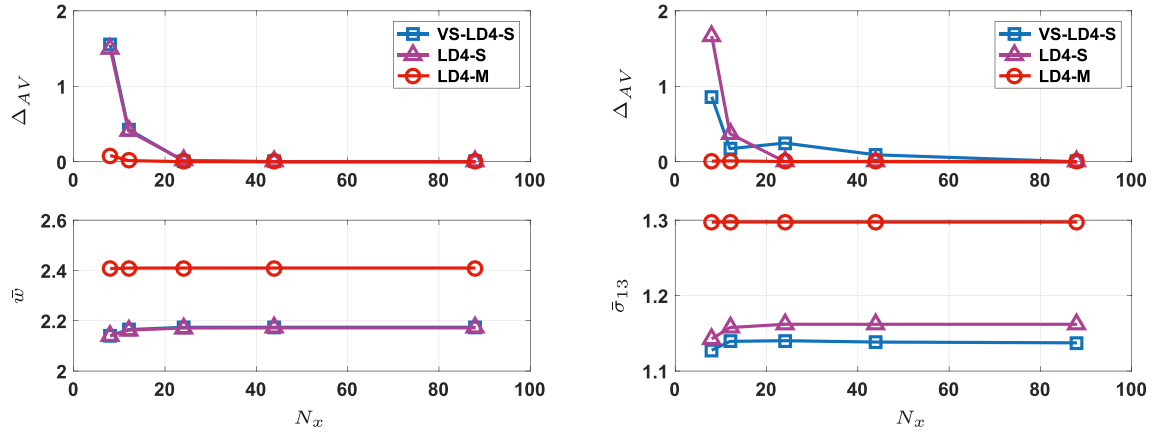

Fig. 4. convergence study - S = 4 - $\varphi = \pi/2$–3 layers [0°/90°/0°].

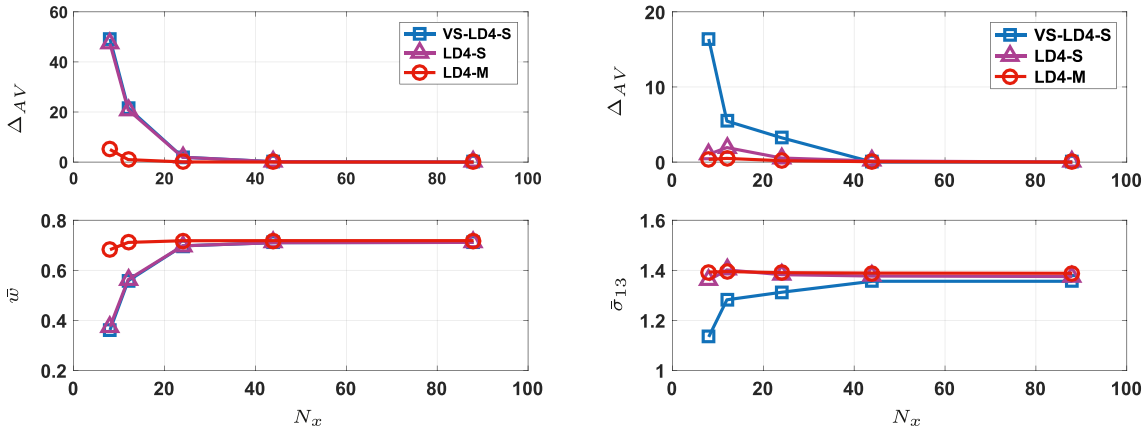

Fig. 5. convergence study - S = 50 - $\varphi = \pi/2$–3 layers [0°/90°/0°].

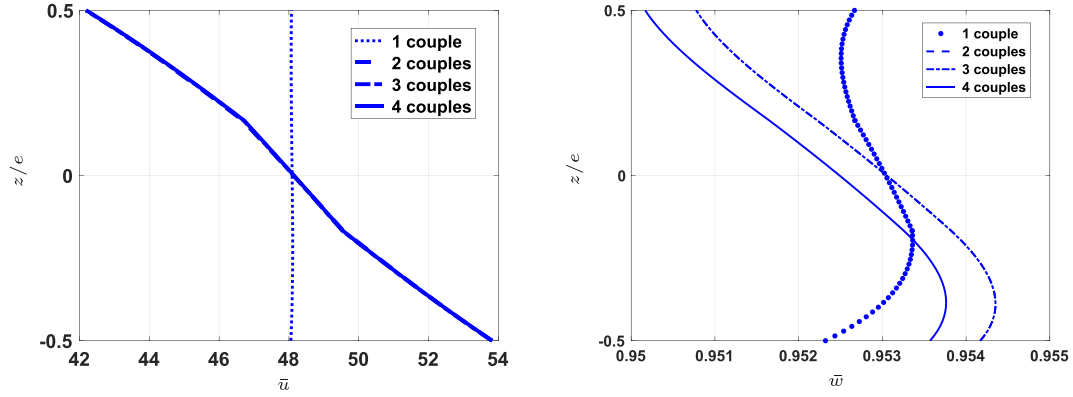

Fig. 6. distribution of $\overline{u}$ (left), $\overline{w}$ (right) along the thickness - convergence study on the couples - S = 10 - $\varphi = \pi/2$–3 layers [0°/90°/0°] - VS-LD4-S model.

geometry: composite cross-ply cylindrical shell, $R = 10$, $\varphi = \pi/2$, constituted of 3, 6, 9, 24 layers (alternating layers at 0° and 90°). All layers have the same thickness. $S = \frac{R}{e} \in \{4, 10, 20, 100\}$. The panel is supposed infinite along the $x_2 = \xi^2$ direction ($b_C = 8a_C$) (Cf. Fig. 3).

boundary conditions: simply-supported shell along its straight edges, subjected to a constant pressure along the curvature: $q(\xi^1) = q_0$

material properties: $E_L = 25$ GPa , $E_T = 1$ GPa , $G_{LT} = 0.2$ GPa, $G_{TT} = 0.5$ GPa , $\nu_{LT} = \nu_{TT} = 0.25$

where L refers to the fiber direction, T refers to the transverse direction.

mesh: only a quarter of the structure is meshed. A space ratio is considered in these two directions (ratio between the size of the larger and the smaller element). Different meshes are considered. See Fig. 3 for instance ($N_x = 44$, $N_y = 10$ with a space ratio of 8).

numerical layers: N_z is the total number of numerical layers.

number of dofs for VS-LD4-S: $Ndof_{xy} = 3(N_x + 1)(N_y + 1)$ and $Ndof_z = 12 \times \alpha NC + 3$ are the number of dofs of the two problems associated with v_j^i and f_j^i respectively. α is the number of numerical layers per physical layer. So the total number of dofs is $Ndof_{xy} + Ndof_z$.

number of dofs for LD4-S: $N_{LW} = 3.(4.N_z + 1).(3.N_x.N_y + 2(N_x + N_y) + 1)$

results: The results are made nondimensional using: $\overline{u} = u_1(a_C/2, b_C/2, z)\frac{E_T}{eq_0S^3}$, $\overline{w} = u_3(0, b_C/2, z)\frac{100E_T}{eq_0S^4}$. $\overline{\sigma}_{\alpha\alpha} = \frac{\sigma_{\alpha\alpha}(0,b_C/2,z)}{q_0S^2}$,. $\overline{\sigma}_{13} = \frac{\sigma_{13}(a_C/2,b_C/2,z)}{q_0S}$, $\overline{\sigma}_{33} = \frac{\sigma_{33}(0,b_C/2,z)}{q_0}$

An error rate is defined as

$$\Delta_{AV} = 100\frac{|x - x_{AV}|}{|x_{AV}|} \text{ where } x = \overline{w}, \overline{\sigma}_{13} \tag{43}$$

the subscript $_{AV}$ stands for the asymptotic value (corresponding to the refined mesh).

First of all, a convergence study is performed for the three approaches (Figs. 4 and 5). A three-layer configuration with two slenderness ratios (thick and thin shells) is considered. The variations of the transverse displacement, the transverse shear stress and the error rate Δ_{AV} (Eq. (43)) with respect to the number of elements along the ξ axis are reported in these figures. A mesh with a space ratio equal to 8 in the

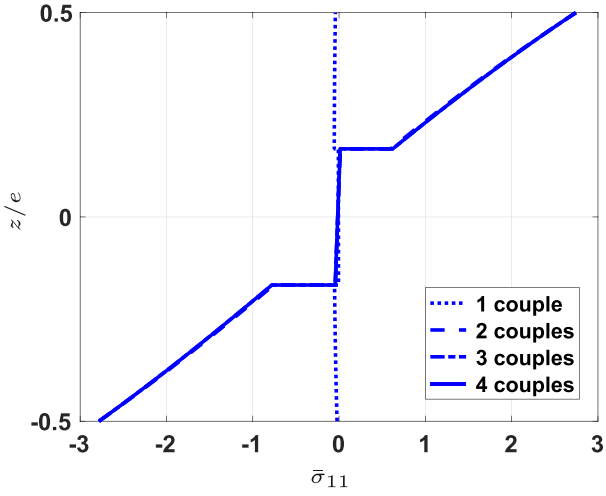

Fig. 7. distribution of $\overline{\sigma}_{11}$ along the thickness - convergence study on the couples - S = 10 - $\varphi = \pi/2$–3 layers [0°/90°/0°] - VS-LD4-S model.

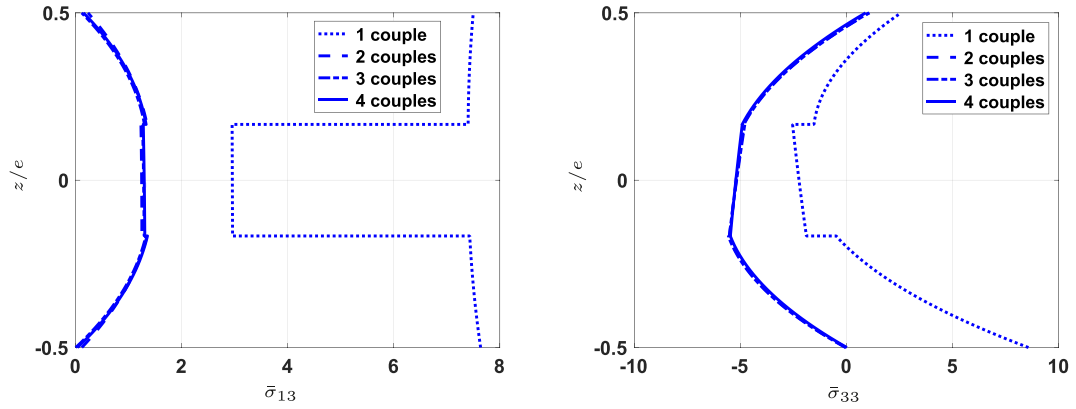

Fig. 8. distribution of $\overline{\sigma}_{13}$ (left) and $\overline{\sigma}_{33}$ (right) along the thickness - convergence study on the couples - S = 10 - $\varphi = \pi/2$–3 layers [0°/90°/0°] - VS-LD4-S model.

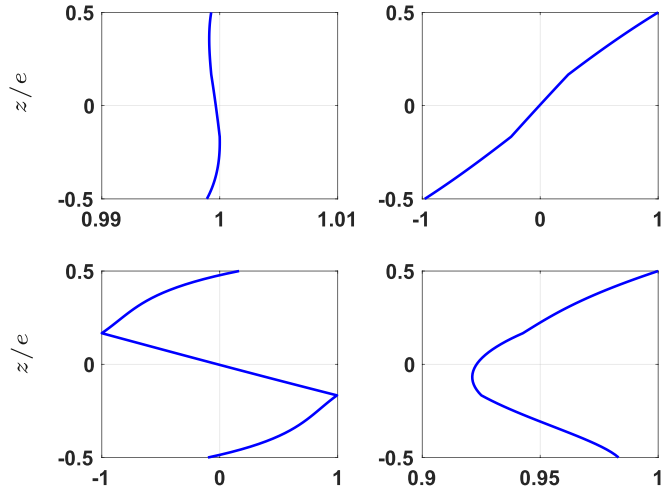

Fig. 9. distribution of f_1^i $(i = 1, 2, 3, 4)$ along the thickness - S = 10 - $\varphi = \pi/2$–3 layers [0°/90°/0°] - VS-LD4-S model.

two directions is used. It can be inferred from these results that the convergence rate of the shell theory (LD4-M model) is better than the other one (the degenerated shell). As it will be discussed in the subsequent examples, the asymptotic value is different for the thick case between the LD4-M and LD4-S models due to the approximation of the geometry of the degenerated shell approach. We can also notice that the variable separation drives to the same results for the displacement. As far as the transverse shear stress is concerned, the convergence rate is different, but the asymptotic value is very close.

Based on this study, a 44 × 10 mesh will be used in the following.

Then, the study is focused on the VS-LD4-S model in order to illustrate the behavior of the PGD method. A three-layer shell with $S = 10$ is considered. The behavior of the method is given in Figs. 6–8. These figures show the convergence of the PGD process on both displacements and stresses. The two first couples allow us to build a solution very close to the converged one. The following couples bring only small corrections on the transverse stresses.

For further illustration, the functions $f_1^i(z)$ are given in Fig. 9. The two first functions are constant and linear, corresponding to classical models (FSDT). Then, the distribution of the two other couples is more complex, they represent small contributions to the whole solution.

The present method is also assessed for different slenderness ratios, from thick to thin shell. In Table 2, the results are compared with the LD4-S approach for displacements, in-plane and transverse stresses.

Table 2
Comparison VS-LD4-S/LD4-S - [0°/90°/0°] - $\varphi = \pi/2$ - $N_z = NC$.

S		$\overline{u}(e/2)$	$\overline{w}(0)$	$\overline{\sigma}_{11}(-e/2)$	$\overline{\sigma}_{13}(0)$	$\overline{\sigma}_{33}$max
4	VS-LD4-S	36.2634 (0.0%)	2.1742 (0.1%)	−3.6118 (0.4%)	1.1382 (2.0%)	−1.8696 (0.8%)
	LD4-S	36.2520	2.1716	−3.5966	1.1620	−1.8843
10	VS-LD4-S	42.1928 (0.0%)	0.9525 (0.1%)	−2.7815 (0.3%)	1.2939 (1.0%)	−5.4830 (0.9%)
	LD4-S	42.1756	0.9519	−2.7732	1.3065	−5.5322
20	VS-LD4-S	71.3874 (0.0%)	0.7651 (0.0%)	−2.6405 (0.1%)	1.3191 (2.3%)	−11.6381 (1.0%)
	LD4-S	71.3923	0.7648	−2.6391	1.3507	−11.7616
100	VS-LD4-S	344.2876 (0.1%)	0.6877 (0.0%)	−2.5798 (0.0%)	1.3709 (0.9%)	−57.0588 (0.2%)
	LD4-S	344.5605	0.6878	−2.5794	1.3837	−56.9431

Table 3
Comparison VS-LD4-S/LD4-M - [0°/90°/0°] - $\varphi = \pi/2$ - $N_z = NC$.

S		$\overline{u}(h/2)$	$\overline{w}(0)$	$\overline{\sigma}_{11}(-h/2)$	$\overline{\sigma}_{13}(0)$	$\overline{\sigma}_{33}$max
4	VS-LD4-S	36.2634 (10.0%)	2.1742 (9.8%)	−3.6118 (21.3%)	1.1382 (12.3%)	−1.8696 (17.5%)
	LD4-M	40.2734	2.4097	−4.5877	1.2974	−2.2653
10	VS-LD4-S	42.1928 (4.4%)	0.9525 (4.4%)	−2.7815 (8.3%)	1.2939 (5.6%)	−5.4830 (5.5%)
	LD4-M	44.1184	0.9968	−3.0331	1.3702	−5.8036
20	VS-LD4-S	71.3874 (2.3%)	0.7651 (2.3%)	−2.6405 (4.1%)	1.3191 (4.7%)	−11.6381 (0.3%)
	LD4-M	73.1034	0.7834	−2.7547	1.3841	−11.6040
100	VS-LD4-S	344.2876 (0.2%)	0.6877 (1.6%)	−2.5798 (0.7%)	1.3709 (1.2%)	−57.0588 (0.7%)
	LD4-M	345.0776	0.6990	−2.5981	1.3875	−57.4470

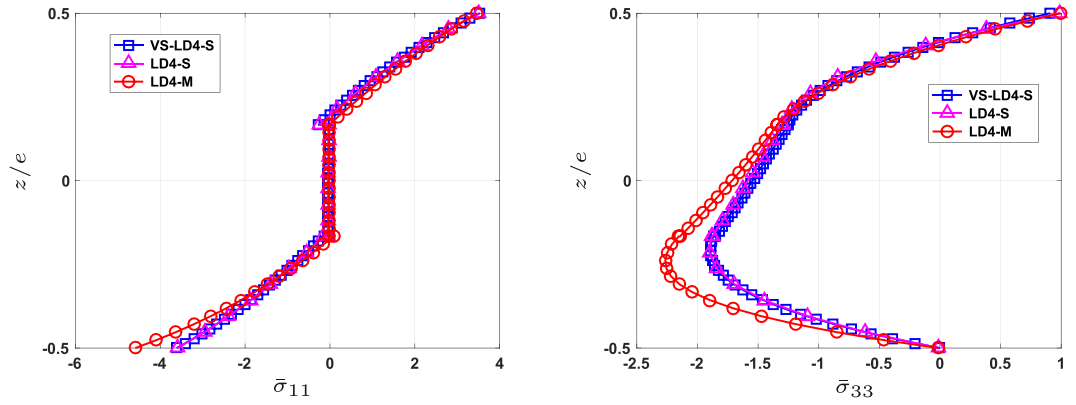

Fig. 10. distribution of $\overline{\sigma}_{11}$ (left) and $\overline{\sigma}_{33}$ (right) along the thickness - S = 4 - 3 layers.

Table 4
Comparison VS-LD4-S/LD4-M - $\varphi = \pi/2$ - $S = 10$ - $N_z = NC$.

NC		$\overline{u}(e/2)$	$\overline{w}(0)$	$\overline{\sigma}_{11}(-e/2)$	$\overline{\sigma}_{13\ max}$	$\overline{\sigma}_{33max}$
6	VS-LD4-S	70.8408 (2.7%)	1.6747 (2.6%)	−4.4873 (7.3%)	1.5219 (4.6%)	−5.9020 (5.6%)
	LD4-M	72.7697	1.7194	−4.8381	1.5954	−6.2529
9	VS-LD4-S	54.1182 (4.4%)	1.2318 (4.5%)	−3.7848 (8.7%)	1.3624 (3.3%)	−5.2850 (6.4%)
	LD4-M	56.6165	1.2895	−4.1451	1.4096	−5.6479
24	VS-LD4-S	67.3724 (4.0%)	1.5552 (4.0%)	−4.7467 (8.6%)	1.4873 (3.1%)	−5.8211 (4.0%)
	LD4-M	70.1935	1.6203	−5.1951	1.5355	−6.0636

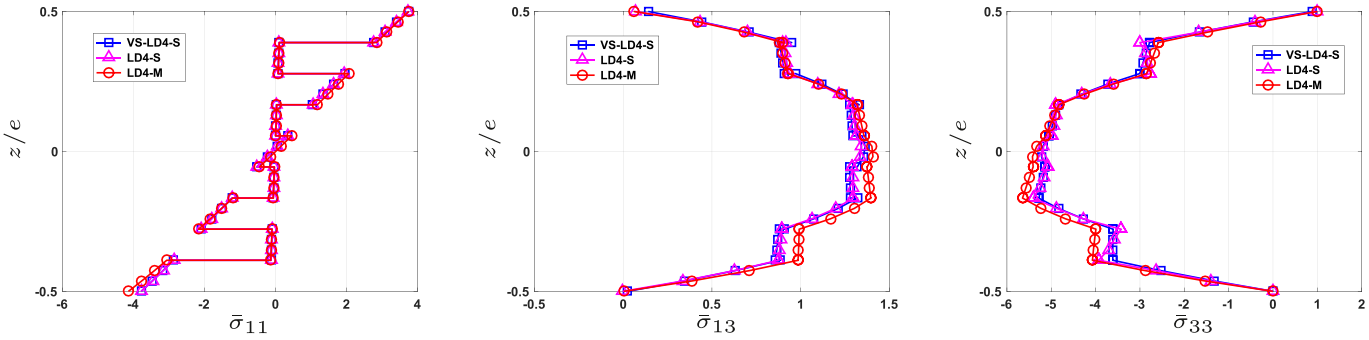

Fig. 11. distribution of $\overline{\sigma}_{11}$ (left), $\overline{\sigma}_{13}$ (middle) and $\overline{\sigma}_{33}$ (right) along the thickness - S = 10 - 9 layers.

Two, three or four couples are built depending on the slenderness ratio. The excellent agreement with the LD4-S model shows that the variable separation does not introduce additional errors for the solution regardless of the value of S.

The results are also compared with the LD4-M model (cf. Table 3). It can be inferred from this table that the slenderness ratio has an influence on the results. For very thick case, the simplified assumption on the geometry of the shell drives to a significant error rate (from 10 to 21%). For further illustration, Fig. 10 shows the distribution of the in-plane and transverse normal stresses through the thickness at the center of the structure. The main difference between the two approaches occurs at the bottom of the shell. Nevertheless, we can notice that the present method can be applied for semi-thick to thin structures as the error rate becomes acceptable.

Finally, the approach is assessed on a semi-thick shell ($S = 10$) for different numbers of layers ($NC = 6, 9, 24$). The choice of this configuration comes from the previous analysis where the error rate remains good. From Table 4, we can notice that the error rate is less than 4.5% for the displacements and 8.7% for the stresses when compared with the reference solution. Through-thickness distribution of stresses for a 9-layer configuration are also plotted in Fig. 11. The present distributions are in excellent agreement with the LD4-S model and the accuracy of this approach is very good with respect to the reference solution. Equivalent Single models fail to model shell structures with these stacking sequences.

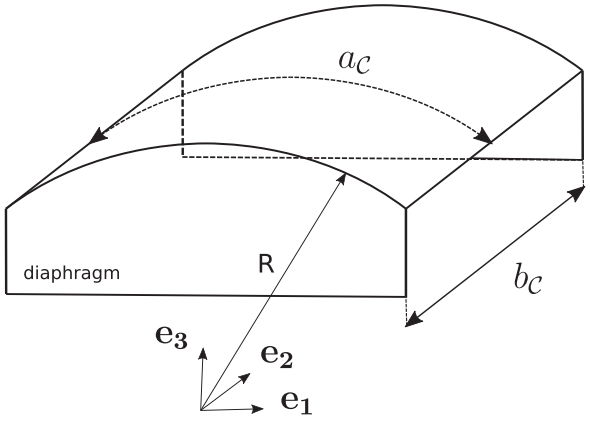

Fig. 12. shell panel with rigid diaphragm.

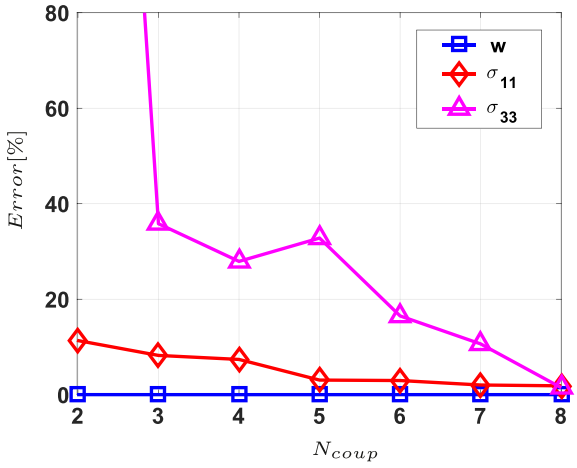

Fig. 13. distribution of the error with respect to the number of couples - NC = 3 - rigid diaphragm - S = 20 - $R/a_C = 2$

6.2. Shell panel with rigid diaphragm

In this section, the present test involves a shell panel with a rigid diaphragm. The main characteristics are given as follows

geometry: composite cross-ply shell panel, $R = 3$, $b_C = 6$, different values of parameter $R/a_C \in \{1, 2, 10, 20\}$, constituted of 3 layers $[0°/90°/0°]$. $S = 10, 20$. All layers have the same thickness. See Fig. 12.
boundary conditions: rigid diaphragm along its curved edges, subjected to a constant pressure on the top surface along the curvature: q_0
material properties: same materials as in Section 6.1
mesh: only a quarter of the structure is meshed ($N_x = N_y = 24$ with a space ratio of 5)
numerical layers: N_z is the total number of numerical layers.
number of dofs for VS-LD4-S: $Ndof_{xy} = 1875$ and $Ndof_z = 12 \times \alpha NC + 3$

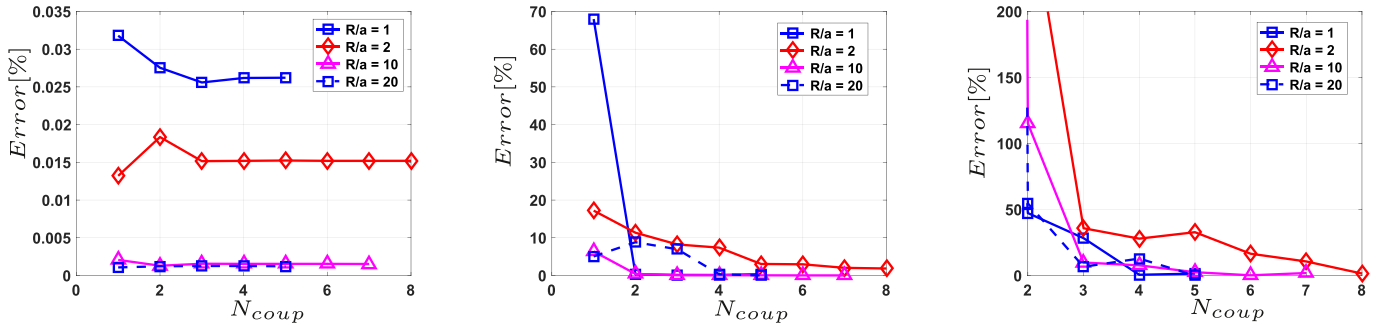

(a) $\bar{w}$ (b) $\bar{\sigma}_{11}$ (c) $\bar{\sigma}_{33}$

Fig. 14. distribution of the error with respect to the number of couples for different values of R/a_C - NC = 3 - rigid diaphragm - S = 20.

Table 5
Comparison VS-LD4-S/LD4-S - rigid diaphragm - $NC = 3$.

S	R/a_C	$\overline{w}(0)$				$\overline{\sigma}_{11}(-h/2)$				$\overline{\sigma}_{33}$max			
		1	2	10	20	1	2	10	20	1	2	10	20
10	VS-LD4-S	2.6959	9.6849	13.4178	13.4262	0.5298	−0.1752	0.1295	−0.2346	1.2231	1.1980	1.5897	1.5719
	Err-LD4-S	0.00%	0.00%	0.00%	0.00%	0.60%	1.29%	0.24%	1.20%	2.48%	2.24%	4.68%	3.31%
	LD4-S	2.6959	9.6852	13.4173	13.4259	0.5330	−0.1775	0.1292	−0.2374	1.1934	1.1718	1.5187	1.6256
20	VS-LD4-S	0.7776	5.1578	13.2319	13.2689	0.4250	0.1157	0.1337	0.1256	1.8421	1.4076	2.5579	2.4259
	Err-LD4-S	0.00%	0.01%	0.00%	0.00%	0.29%	2.55%	0.05%	0.02%	2.71%	19.72%	11.12%	0.36%
	LD4-S	0.7776	5.1581	13.2324	13.2693	0.4262	0.1128	0.1336	0.1257	1.8934	1.1757	2.3019	2.4348

Table 6
Comparison VS-LD4-S/LD4-S/LD4-M - rigid diaphragm - $NC = 3$ - $f_i(z)$ updated.

S	R/a_C	$\overline{w}(0)$				$\overline{\sigma}_{11}(-h/2)$				$\overline{\sigma}_{33}$max			
		1	2	10	20	1	2	10	20	1	2	10	20
10	VS-LD4-S	2.6971	9.6868	13.4184	13.4266	0.5306	−0.1826	0.1293	−0.2365	1.2152	1.1658	1.5307	1.6107
	Err-LD4-S	0.04%	0.02%	0.01%	0.00%	0.44%	2.85%	0.13%	0.40%	1.82%	0.51%	0.79%	0.92%
	Err-LD4-M	4.80%	4.84%	4.78%	4.78%	3.30%	6.71%	3.74%	2.42%	1.50%	2.66%	0.22%	3.59%
	LD4-S	2.6959	9.6852	13.4173	13.4259	0.5330	−0.1775	0.1292	−0.2374	1.1934	1.1718	1.5187	1.6256
	LD4-M	2.8331	10.1792	14.0916	14.1006	0.5487	0.1711	0.1344	−0.2424	1.1972	1.1356	1.5274	1.6706
20	VS-LD4-S	0.7778	5.1588	13.2326	13.2695	0.4247	0.1159	0.1336	0.1257	1.9206	1.2228	2.3452	2.4346
	Err-LD4-S	0.03%	0.02%	0.00%	0.00%	0.35%	1.86%	0.02%	0.02%	1.44%	1.48%	1.88%	0.01%
	Err-LD4-M	2.44%	2.49%	2.47%	2.46%	2.46%	9.41%	1.90%	1.97%	0.33%	6.66%	3.98%	1.18%
	LD4-S	0.7776	5.1581	13.2324	13.2693	0.4262	0.1128	0.1336	0.1257	1.8934	1.1757	2.3019	2.4348
	LD4-M	0.7972	5.2905	13.5671	13.6046	0.4354	0.1050	0.1362	0.1282	1.9142	1.1185	2.2555	2.4061

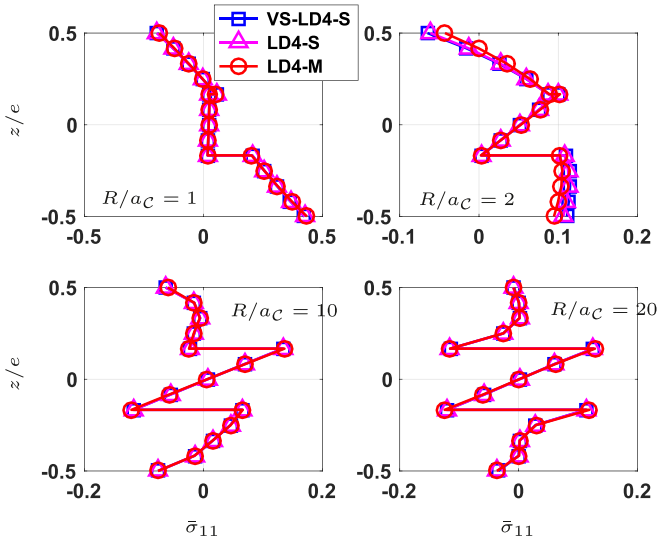

Fig. 15. distribution of $\overline{\sigma}_{11}$ through the thickness - NC = 3 - rigid diaphragm - S = 20.

number of dofs for LD4-S: $N_{LW} = 71175$ for $N_z = 3$, $N_{LW} = 136875$ for $N_z = 6$
results: The results are made nondimensional using: $\overline{w} = u_3(a_C/2, b_C/2, z)\frac{100E_T}{eq_0S^4}$. $\overline{\sigma}_{\alpha\alpha} = \frac{\sigma_{\alpha\alpha}(a_C/2,b_C/2,z)}{q_0S^2}$,. $\overline{\sigma}_{33} = \frac{\sigma_{33}(a_C/2,b_C/2,z)}{q_0}$
reference solution: LD4-M model

For this test case, different values of the parameter R/a_C are considered referring to deep or shallow shells. The convergence in terms of number of couples is given in Fig. 13 for $S = 20$, $R/a_C = 2$. A high convergence rate is found for the transverse displacement, while more couples are needed to obtain the transverse normal stress with accuracy. For this configuration, eight couples are built. Further illustrations are shown in Fig. 14 where different values of R/a_C are considered. The previous remark remains true. The convergence rate of the different mechanical quantities is not the same. A small error rate is obtained for the transverse displacement with few couples, that is not the case for σ_{33}. Moreover, it can be noticed that the configuration with $R/a_C = 2$ seems to be the most severe case for this example.

Numerical results are also summarized in Table 5 where the two present approaches are compared for two slenderness ratios. The results are in very good agreement for the transverse displacements and the in-plane stress. But, a substantial error can be noted for the transverse stress. As in Ref. [43], it can be reduced by updating the z-functions f_i. This is achieved efficiently (see Table 6), and the maximum error rate for $\overline{\sigma}_{33}$ decreases from 19% to 1.8%. The results can be also compared with the reference solution (LD4-M). The displacement drives to a maximum error rate of 4.9%, while the maximal error rate on the stresses is 9%. It is related to the case $R/a_C = 2$. This error comes from the assumptions on the geometry of the shell. To show the wide range of configurations involved in this test, Fig. 15 illustrates the

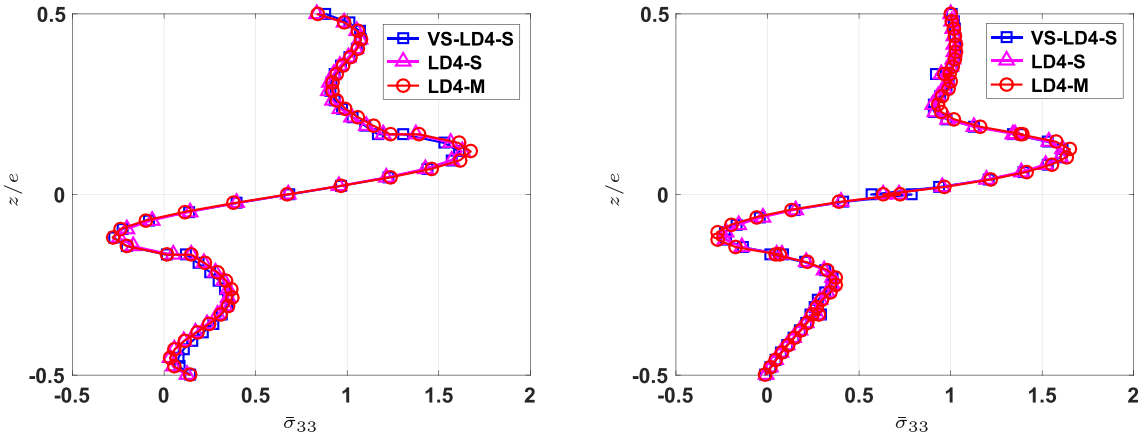

Fig. 16. distribution of $\overline{\sigma}_{33}$ along the thickness - $N_z = 3$ (left)/$N_z = 6$ (right) numerical layers - NC = 3 - rigid diaphragm - S = 10 - $R/a_C = 20$

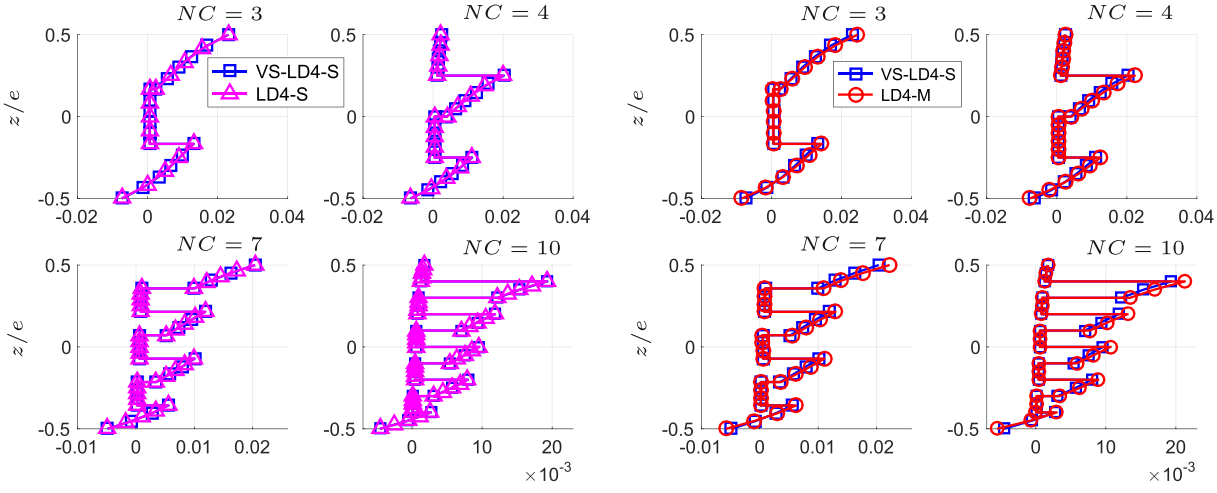

Fig. 17. distribution of $\overline{\sigma}_{11}$ along the thickness - $NC = 3/4/7/10$ - spherical shell - $R/a_C = 5$

various distributions of the in-plane stress through the thickness for $R/a_C = 1, 2, 10, 20$. Despite the complexity of these distributions, the present approach drives to satisfactory results when compared with the reference solution.

Another aspect is addressed in Fig. 16. For $S = 10$ and $R/a_C = 20$, oscillations in the first and third layers occur in the distribution of the transverse normal stress (Fig. 16 left). It can be overcome by introducing numerical layers in each physical layer ($N_z = 6$). The new results are given in Fig. 16 right. As the problem to be solved is split into an in-plane/out-of-plane problem, it does not affect the computational cost of the method as in Refs. [42,43]. Note that the same phenomenon occurs for the in-plane stress, but it is not shown for brevity reason.

6.3. Spherical shell

A doubly-curved laminated composite structure is considered in this section. The test is described as follows

geometry: spherical square composite cross-ply shell, $R = 3$, $R/a_C = 5$, with 3/4/7/10 layers. $S = 25$. All the layers have the same thickness.
boundary conditions: clamped shell on all edges, subjected to a constant pressure q_0
material properties: same materials as in Section 6.1
mesh: only a quarter of the structure is meshed. $N_x = 24, N_y = 24$
number of dofs for VS-LD4-S: $Ndof_{xy} = 1875$ and $Ndof_z = 12 \times NC + 3$. $Ndof_z = 39$ to $Ndof_z = 123$ (3/10 layers)
number of dofs for LD4-S: $N_{LW} = 71175$ for $N_z = 3$, $N_{LW} = 224475$ for $N_z = 10$
results: The results are made nondimensional using: $\overline{\sigma}_{11} = \frac{\sigma_{11}(a_C/2, b_C/2, z)}{q_0 S^2}$,
reference solution: LD4-M model

The distribution of σ_{11} along the thickness at the center of the shell is given in Fig. 17 for different numbers of layers. Seven couples are computed for VS-LD4-S model. It can be inferred from this figure that the results of the present approaches are in very good agreement with the reference solution. For such structures, the use of variable separation does not affect the accuracy of the results (Fig. 17 left). Moreover, the number of unknowns involved in the VS-LD4-S model remains low despite the increase of the number of layers.

7. Conclusion

In this article, two degenerated shell approaches are applied in conjunction with a LayerWise approach and a variable separation method for the modeling of composite structures. A fourth-order LW description of the displacements is used. The two models are assessed through a wide range of configurations involving different geometries, stacking sequences and boundary conditions. The results are compared with a reference solution which comes from a model available in open literature. Accurate results have been obtained despite the assumptions on the geometry of the shell. The approaches have the capability to model semi-thick to thin structures. Moreover, if needed, numerical layers in each physical layer can be introduced without increasing significantly the computational cost for the model based on the variable separation.

Based on these promising results, the membrane and shear locking phenomenon will be addressed in future investigation.

Author statement

P. Vidal: Software, Conceptualization, Methodology, Writing-Original draft. L. Gallimard: Methodology, Writing – Review & Editing. O. Polit: Methodology, Conceptualization, Writing – Review & Editing.

Declaration of competing interest

The authors declare that they have no known competing financial interests or personal relationships that could have appeared to influence the work reported in this paper.

Appendix A. Finite element problem to be solved on Ω

Appendix A.1. Expression of $\mathbf{BaseTA}_\square$ and $\mathbf{\Sigma}_{\mathbf{z}}^{\square}(\widetilde{f})$

$$\mathbf{BaseTA_p} = \begin{bmatrix} \mathbf{TA_{p1}} & \mathbf{0}_{3\times1} & \mathbf{0}_{3\times1} \\ \mathbf{0}_{3\times1} & \mathbf{TA_{p2}} & \mathbf{0}_{3\times1} \\ \mathbf{0}_{3\times1} & \mathbf{0}_{3\times1} & \mathbf{TA_{p3}} \end{bmatrix} \tag{A.1}$$

with

$$\mathbf{TA_{pi}} = \mathbf{t_1} \cdot \mathbf{e_i} \begin{bmatrix} \mathbf{t_1} \cdot \mathbf{a_1}\ \mathbf{N}_{\xi,\xi} & & \\ \mathbf{t_1} \cdot \mathbf{a_2}\ \mathbf{N}_{\xi,\eta} & & \\ \mathbf{t_1} \cdot \mathbf{a_1}\ \mathbf{N}_{\xi,\eta} + \mathbf{t_1} \cdot \mathbf{a_2}\ \mathbf{N}_{\xi,\xi} & & \end{bmatrix} + \mathbf{t_2} \cdot \mathbf{e_i} \begin{bmatrix} \mathbf{t_2} \cdot \mathbf{a_1}\ \mathbf{N}_{\xi,\xi} & & \\ \mathbf{t_2} \cdot \mathbf{a_2}\ \mathbf{N}_{\xi,\eta} & & \\ \mathbf{t_2} \cdot \mathbf{a_1}\ \mathbf{N}_{\xi,\eta} + \mathbf{t_2} \cdot \mathbf{a_2}\ \mathbf{N}_{\xi,\xi} & & \end{bmatrix}, \quad i = 1, 2, 3$$

$$\mathbf{BaseTA_n} = \begin{bmatrix} \mathbf{t_3} \cdot \mathbf{e_1}\ \mathbf{N}_\xi & 0 & 0 \\ 0 & \mathbf{t_3} \cdot \mathbf{e_2}\ \mathbf{N}_\xi & 0 \\ 0 & 0 & \mathbf{t_3} \cdot \mathbf{e_3}\ \mathbf{N}_\xi \end{bmatrix} \tag{A.2}$$

$$\mathbf{BaseTA_{s1}} = \begin{bmatrix} \boldsymbol{TA_{s11}} & \mathbf{0}_{2\times1} & \mathbf{0}_{2\times1} \\ \mathbf{0}_{2\times1} & \boldsymbol{TA_{s12}} & \mathbf{0}_{2\times1} \\ \mathbf{0}_{2\times1} & \mathbf{0}_{2\times1} & \boldsymbol{TA_{s13}} \end{bmatrix} \tag{A.3}$$

with

$$\mathbf{TA_{s1i}} = \mathbf{t_3} \,.\, \mathbf{e_i} \begin{bmatrix} \mathbf{N}_{\xi,\eta} \\ \mathbf{N}_{\xi,\xi} \end{bmatrix}, \quad i = 1,2,3$$

$$\mathbf{BaseTA_{s3}} = \begin{bmatrix} \boldsymbol{TA_{s31}} & \mathbf{0}_{2\times1} & \mathbf{0}_{2\times1} \\ \mathbf{0}_{2\times1} & \boldsymbol{TA_{s32}} & \mathbf{0}_{2\times1} \\ \mathbf{0}_{2\times1} & \mathbf{0}_{2\times1} & \boldsymbol{TA_{s33}} \end{bmatrix} \tag{A.4}$$

with

$$\mathbf{TA_{s3i}} = \mathbf{t_1} \,.\, \mathbf{e_i} \begin{bmatrix} \mathbf{t_1} \,.\, \mathbf{a_2} & \mathbf{N}_\xi \\ \mathbf{t_1} \,.\, \mathbf{a_1} & \mathbf{N}_\xi \end{bmatrix} + \mathbf{t_2} \,.\, \mathbf{e_i} \begin{bmatrix} \mathbf{t_2} \,.\, \mathbf{a_2} & \mathbf{N}_\xi \\ \mathbf{t_2} \,.\, \mathbf{a_1} & \mathbf{N}_\xi \end{bmatrix}, \quad i = 1,2,3$$

$$\boldsymbol{\Sigma}_{\mathbf{z}}^{\mathbf{p}}(\widetilde{f}) = \left[\widetilde{f}_1 \, \mathbf{Id}_{3\times3} \;\vdots\; \widetilde{f}_2 \, \mathbf{Id}_{3\times3} \;\vdots\; \widetilde{f}_3 \, \mathbf{Id}_{3\times3} \right] \tag{A.5}$$

$$\boldsymbol{\Sigma}_{\mathbf{z}}^{\mathbf{n}}(\widetilde{f}) = \left[\widetilde{f}'_1 \;\vdots\; \widetilde{f}'_2 \;\vdots\; \widetilde{f}'_3 \right] \tag{A.6}$$

$$\boldsymbol{\Sigma}_{\mathbf{z}}^{\mathbf{s1}}(\widetilde{f}) = \left[\widetilde{f}_1 \, \mathbf{Id}_{2\times2} \;\vdots\; \widetilde{f}_2 \, \mathbf{Id}_{2\times2} \;\vdots\; \widetilde{f}_3 \, \mathbf{Id}_{2\times2} \right] \tag{A.7}$$

$$\boldsymbol{\Sigma}_{\mathbf{z}}^{\mathbf{s3}}(\widetilde{f}) = \left[\widetilde{f}'_1 \, \mathbf{Id}_{2\times2} \;\vdots\; \widetilde{f}'_2 \, \mathbf{Id}_{2\times2} \;\vdots\; \widetilde{f}'_3 \, \mathbf{Id}_{2\times2} \right] \tag{A.8}$$

where $\mathbf{Id}_{i\times i}$ is the $i \times i$ identity matrix.

Appendix A.2. Expression of $\boldsymbol{\Sigma}^{\square}_{\boldsymbol{new}}(\widetilde{f})$ and $\boldsymbol{MM}^{p}_{LR}$

$$\boldsymbol{\Sigma}_{\mathbf{new}}^{\mathbf{p}}(\widetilde{f}) = \boldsymbol{\Sigma}_{\mathbf{z}}^{\mathbf{p}}(\widetilde{f}) \tag{A.9}$$

$$\mathbf{MM}^{p}_{LR} = \begin{bmatrix} \mathbf{TT}_{LR} & \mathbf{0}_{3\times3} & \mathbf{0}_{3\times3} \\ \mathbf{0}_{3\times3} & \mathbf{TT}_{LR} & \mathbf{0}_{3\times3} \\ \mathbf{0}_{3\times3} & \mathbf{0}_{3\times3} & \mathbf{TT}_{LR} \end{bmatrix} \tag{A.10}$$

Appendix B. Finite element problem to be solved on $\Omega_{\boldsymbol{z}}$

*Appendix B.1. Expression of **BaseNz** and **BaseBz***

$$\mathbf{BaseNz} = \begin{bmatrix} \mathbf{N}_z & 0 & 0 \\ 0 & \mathbf{N}_z & 0 \\ 0 & 0 & \mathbf{N}_z \end{bmatrix} \tag{B.1}$$

$$\mathbf{BaseBz} = \begin{bmatrix} \mathbf{N}_{z,z} & 0 & 0 \\ 0 & \mathbf{N}_{z,z} & 0 \\ 0 & 0 & \mathbf{N}_{z,z} \end{bmatrix} \tag{B.2}$$

Appendix B.2Expression of $\boldsymbol{\Sigma}^{\square}_{\boldsymbol{xy}}(\widetilde{\nu})$

$$\boldsymbol{\Sigma}_{\mathbf{xy}}^{\mathbf{p}}(\widetilde{\nu}) = \begin{bmatrix} tta_{11}\,\widetilde{\nu}_{1,\xi} & tta_{12}\,\widetilde{\nu}_{2,\xi} & tta_{13}\,\widetilde{\nu}_{3,\xi} \\ tta_{21}\,\widetilde{\nu}_{1,\eta} & tta_{22}\,\widetilde{\nu}_{2,\eta} & tta_{23}\,\widetilde{\nu}_{3,\eta} \\ tta_{11}\,\widetilde{\nu}_{1,\eta} + tta_{21}\,\widetilde{\nu}_{1,\xi} & tta_{12}\,\widetilde{\nu}_{2,\eta} + tta_{22}\,\widetilde{\nu}_{2,\xi} & tta_{13}\,\widetilde{\nu}_{3,\eta} + tta_{23}\,\widetilde{\nu}_{3,\xi} \end{bmatrix} \tag{B.3}$$

with $tta_{ij} = \boldsymbol{t_1}.\boldsymbol{e_j}\boldsymbol{t_1}.\boldsymbol{a_i} + \boldsymbol{t_2}.\boldsymbol{e_j}\boldsymbol{t_2}.\boldsymbol{a_i}$

$$\boldsymbol{\Sigma}^{\mathbf{n}}_{\mathbf{xy}}(\widetilde{\nu}) = \begin{bmatrix} \mathbf{t_3} \cdot \mathbf{e_1}\, \widetilde{\nu}_1 & \mathbf{t_3} \cdot \mathbf{e_2}\, \widetilde{\nu}_2 & \mathbf{t_3} \cdot \mathbf{e_3}\, \widetilde{\nu}_3 \end{bmatrix} \tag{B.4}$$

$$\boldsymbol{\Sigma}^{\mathbf{s1}}_{\mathbf{xy}}(\widetilde{\nu}) = \begin{bmatrix} \mathbf{t_3} \cdot \mathbf{e_1}\, \widetilde{\nu}_{1,\eta} & \mathbf{t_3} \cdot \mathbf{e_2}\, \widetilde{\nu}_{1,\eta} & \mathbf{t_3} \cdot \mathbf{e_3}\, \widetilde{\nu}_{1,\eta} \\ \mathbf{t_3} \cdot \mathbf{e_1}\, \widetilde{\nu}_{1,\xi} & \mathbf{t_3} \cdot \mathbf{e_2}\, \widetilde{\nu}_{1,\xi} & \mathbf{t_3} \cdot \mathbf{e_3}\, \widetilde{\nu}_{1,\xi} \end{bmatrix} \tag{B.5}$$

$$\boldsymbol{\Sigma}^{\mathbf{s3}}_{\mathbf{xy}}(\widetilde{\nu}) = \begin{bmatrix} tta_{21}\, \widetilde{\nu}_1 & tta_{22}\, \widetilde{\nu}_2 & tta_{23}\, \widetilde{\nu}_3 \\ tta_{11}\, \widetilde{\nu}_1 & tta_{12}\, \widetilde{\nu}_2 & tta_{13}\, \widetilde{\nu}_3 \end{bmatrix} \tag{B.6}$$

References

[1] M. Bernadou, Finite Element Methods for Thin Shell Problems, John Wiley et Sons, Chichester, 1996.

[2] F. Dau, O. Polit, M. Touratier, A efficient c^1 finite element with continuity requirements for multilayered/sandwich shell structures, Comput. Struct. 82 (2004) 1889–1899.

[3] O. Zienkiewicz, R. Taylor, fifth ed., The Finite Element Method, vol. 2, Butterworth-Heinemann, 2000.

[4] P. Vidal, M. D'Ottavio, M.B. Thaier, O. Polit, An efficient finite shell element for the static response of piezoelectric laminates, J. Intell. Mater. Syst. Struct. 22 (7) (2011) 671–690, https://doi.org/10.1177/1045389X11402863.

[5] J. Reddy, Mechanics of Laminated Composite Plates and Shells – Theory and Analysis, CRC Press Inc, 2004.

[6] A. Leissa, Vibration of Shells, NASA SP-288, Nasa Report, 1973.

[7] C. Jeyachandrabose, J. Kirkhope, Explicit formulation of two anisotropic, triangular, thin, shallow shell elements, Comput. Struct. 25 (1987) 415–436.

[8] K. Rao, A rectangular laminated anisotropic shallow thin shell finite element, Comput. Methods Appl. Mech. Eng. 15 (1978) 13–33.

[9] M. Qatu, A. Leissa, Bending analysis of laminated plates and shells by different methods, Comput. Struct. 52 (1994) 529–539.

[10] S. Hossain, P. Sinha, A. Sheikh, A finite element formulation for the analysis of laminated composite shells, Comput. Struct. 82 (2004) 1623–1638.

[11] G. Sgambitterra, A. Adumitroaie, E. Barbero, A. Tessler, A robust three-node shell element for laminated composites with matrix damage, Compos. B Eng. J. 42 (2011) 41–50.

[12] M. Balah, H. Al-Ghamedy, Finite element formulation of a third order laminated finite rotation shell element, Comput. Struct. 80 (2002) 1975–1990.

[13] T. Kant, M. Menon, Estimation of interlaminar stresses in fibre reinforced composite cylindrical shells, Comput. Struct. 38 (1991) 131–147.

[14] M. Cinefra, E. Carrera, Shell finite elements with different through-the-thickness kinematics for the linear analysis of cylindrical multilayered structures, Int. J. of Non-Newt. Fluid Mech. 93 (2) (2013) 160–182.

[15] H. Murakami, Laminated composite plate theory with improved in-plane responses, J. Applied Mech. ASME 53 (1986) 661–666.

[16] E. Carrera, Developments, ideas and evaluations based upon the reissner's mixed theorem in the modeling of multilayered plates and shells, Appl. Mech. Rev. 54 (2001) 301–329.

[17] B. Brank, On composite shell models with a piecewise linear warping function, Compos. Struct. 59 (2003) 163–171.

[18] K. Bhaskar, T. Varadan, A higher-order theory for bending analysis of laminated shells of revolution, Comput. Struct. 40 (4) (1991) 815–819.

[19] P. Seide, R. Chaudhuri, Triangular finite element for analysis of thick laminated shells, Int. J. Numer. Methods Eng. 24 (8) (1987) 1563–1579.

[20] S. Klinkel, F. Gruttmann, W. Wagner, A continuum based three dimensional shell element for laminated structures, Comput. Struct. 71 (1999) 43–62.

[21] S. Botello, E. Onate, J. Canet, A layer-wise triangle for analysis of laminated composite plates and shells, Comput. Struct. 70 (1999) 635–646.

[22] M. Liu, C. To, Free vibration analysis of laminated composite shell structures using hybrid strain based layerwise finite elements, Finite Elem. Anal. Des. 40 (2003) 83–120.

[23] Y. Basar, Y. Ding, Interlaminar stress analysis of composites: layer-wise shell finite elements including transverse strains, Comp. Eng. 5 (5) (1995) 485–499.

[24] L. Vu-Quoc, X. Tan, Efficient hybrid-eas solid element for accurate stress prediction in thick laminated beams, plates, and shells, Comput. Methods Appl. Mech. Eng. 253 (2013) 337–355.

[25] M. Yasin, S. Kapuria, An efficient layerwise finite element for shallow composite and sandwich shells, Compos. Struct. 98 (2013) 202–214.

[26] M. Shariyat, Non-linear dynamic thermo-mechanical buckling analysis of the imperfect laminated and sandwich cylindrical shells based on a global-local theory inherently suitable for non-linear analyses, Int. J. Non Lin. Mech. 46 (2011) 253–271.

[27] R. Kapania, A review on the analysis of laminated shells, J. Pressure Vessel Technol. 111 (1989) 88–96.

[28] A. Noor, W. Burton, Assessment of computational models for multilayered composite shells, Appl. Mech. Rev. 43 (4) (1990) 67–97.

[29] W. Gilewski, M. Radwanska, A survey of finite element models for the analysis of moderately thick shells, Finite Elem. Anal. Des. 9 (1991) 1–21.

[30] H. Yang, S. Saigal, A. Masud, R. Kapania, A survey of recent shell finite element, Int. J. Numer. Methods Eng. 47 (2000) 101–127.

[31] E. Carrera, Theories and finite elements for multilayered, anisotropic, composite plates and shells, Arch. Comput. Methods Eng. 9 (2) (2002) 87–140.

[32] J. Reddy, R. Arciniega, Shear deformation plate and shell theories: from stavsky to present, Mech. Adv. Mater. Struct. 11 (2004) 535–582.

[33] J. Hohe, L. Librescu, Advances in the structural modeling of elastic sandwich panels, Mech. Adv. Mater. Struct. 11 (4–5) (2004) 395–424.

[34] M. Qatu, E. Asadi, W. Wang, Review of recent literature on static analyses of composite shells: 2000-2010, Open J. Compos. Mater. 2 (2012) 61–86.

[35] P. Vidal, L. Gallimard, O. Polit, Proper generalized decomposition and layer-wise approach for the modeling of composite plate structures, Int. J. Solid Struct. 50 (14–15) (2013) 2239–2250, https://doi.org/10.1016/j.ijsolstr.2013.03.034.

[36] F. Chinesta, A. Ammar, A. Leygue, R. Keunings, An overview of the proper generalized decomposition with applications in computational rheology, J. Non-Newtonian Fluid Mech. 166 (11) (2011) 578–592.

[37] F. Chinesta, A. Ammar, E. Cueto, Recent advances and new challenges in the use of the proper generalized decomposition for solving multidimensional models, Arch. Comput. Methods Eng. 17 (4) (2010) 327–350.

[38] A. Ammar, B. Mokdada, F. Chinesta, R. Keunings, A new family of solvers for some classes of multidimensional partial differential equations encountered in kinetic theory modeling of complex fluids, J. Non-Newtonian Fluid Mech. 139 (2006) 153–176.

[39] O. Allix, P. Vidal, A new multi-solution approach suitable for structural identification problems, Comput. Methods Appl. Mech. Eng. 191 (25–26) (2002) 2727–2758.

[40] E. Pruliere, 3D simulation of laminated shell structures using the proper generalized decomposition, Compos. Struct. 117 (2014) 373–381.

[41] B. Bognet, A. Leygue, F. Chinesta, Separated representations of 3D elastic solutions in shell geometries, –, Adv. Model. Simul. Eng. Sci. 1 (2014) 4.

[42] P. Vidal, L. Gallimard, O. Polit, Shell finite element based on the proper generalized decomposition for the modeling of cylindrical composite structures, Comput. Struct. 132 (2014) 1–11, https://doi.org/10.1016/j.compstruc.2013.10.015.

[43] P. Vidal, L. Gallimard, O. Polit, Multi-resolution strategies for the modeling of composite shell structures based on the variable separation method, Int. J. Numer. Methods Eng. 117 (7) (2019) 778–799, https://doi.org/10.1002/nme.5978.

[44] E. Carrera, Historical review of zig-zag theories for multilayered plates and shells, Appl. Mech. Rev. 56 (3) (2003) 287–308.

[45] M. D'Ottavio, D. Ballhause, T. Wallmersperger, B. Kröplin, Considerations on higher-order finite elements for multilayered plates based on a unified formulation, Comput. Struct. 84 (2006) 1222–1235.

[46] J.G. Ren, Exact solutions for laminated cylindrical shells in cylindrical bending, Compos. Sci. Technol. 29 (1987) 169–187.